LA-UR-15-27241 (Accepted Manuscript)

Van Allen Probes, THEMIS, GOES, and Cluster observations of EMIC waves, ULF pulsations, and an electron flux dropout

Sigsbee, Kriss; Reeves, Geoffrey D.; Kletzing, Craig; MacDowall, Robert; Spence, Harlan; Blake, Bern; Baker, Dan; Green, Janet; Singer, Howard; Carr, C.; Santolik, O.

To be published in: Journal of Geophysical Research: Space Physics

DOI to publisher's version: 10.1002/2014JA020877

Permalink to record: http://permalink.lanl.gov/object/view?what=info:lanl-repo/lareport/LA-UR-15-27241

Van Allen Probes, THEMIS, GOES, and Cluster Observations of EMIC waves, ULF pulsations, and an electron flux dropout

K. Sigsbee[1], C. A. Kletzing[1], C. W. Smith[2], Robert MacDowall[3], Harlan Spence[2], Geoff Reeves[4], J. B. Blake[5], D. N. Baker[6], J. C. Green[7], H. J. Singer[8], C. Carr[9], and O. Santolík[10, 11]

[1]Department of Physics and Astronomy, University of Iowa, Iowa City, Iowa, USA

[2]Institute for Earth, Oceans and Space, University of New Hampshire, Durham, New Hampshire, USA

[3]Planetary Magnetospheres Laboratory, NASA Goddard Space Flight Center, Greenbelt, Maryland, USA

[4]Space and Atmospheric Sciences, NIS-1, Los Alamos National Laboratory, Los Alamos, New Mexico, USA

[5]Aerospace Corporation, El Segundo, California, USA

[6]Laboratory for Atmospheric and Space Physics, University of Colorado, Boulder, Colorado, USA

[7]Space Hazards Applications

[8]Space Weather Prediction Center, National Oceanic and Atmospheric Administration, Boulder, Colorado, USA

[9]Department of Physics, Imperial College, London, United Kingdom

[10]Institute of Atmospheric Physics AS CR, Prague, Czech Republic

[11]Faculty of Mathematics and Physics, Charles University in Prague, Prague, Czech Republic

Corresponding Author: K. Sigsbee, Department of Physics and Astronomy, University of Iowa, Iowa City, IA 52242, USA (kristine-sigsbee@uiowa.edu)

Key Points

Data from 7 spacecraft were analyzed during the 12-14 November 2012 storm

EMIC waves were observed by 5 spacecraft during an electron flux dropout

Both adiabatic and non-adiabatic processes needed to explain electron losses

Abstract

We examined an electron flux dropout during the 12-14 November 2012 geomagnetic storm using observations from seven spacecraft: the two Van Allen Probes, THEMIS-A (P5), Cluster 2, and Geostationary Operational Environmental Satellite (GOES) 13, 14, and 15. The electron fluxes for energies greater than 2.0 MeV observed by GOES 13, 14, and 15 at geosynchronous orbit and by the Van Allen Probes remained at or near instrumental background levels for more than 24 hours from 12-14 November. For energies of 0.8 MeV, the GOES satellites observed two shorter intervals of reduced electron fluxes. The first interval of reduced 0.8 MeV electron fluxes on 12-13 November was associated with an interplanetary shock and a sudden impulse. Cluster, THEMIS, and GOES observed intense He^+ EMIC waves from just inside geosynchronous orbit out to the magnetopause across the dayside to the dusk flank. The second interval of reduced 0.8 MeV electron fluxes on 13-14 November was associated with a solar sector boundary crossing and development of a geomagnetic storm with Dst<-100 nT. At the start of the recovery phase, both the 0.8 and 2.0 MeV electron fluxes finally returned to near pre-storm values, possibly in response to strong ultra-low frequency (ULF) waves observed by the

Van Allen Probes near dawn. A combination of adiabatic effects, losses to the magnetopause, scattering by EMIC waves, and acceleration by ULF waves can explain the observed electron behavior.

Index Terms:
2774 Radiation belts, 2788 Magnetic storms and substorms, 2772 Plasma waves and instabilities, 7867 Wave/particle interactions, 2784 Solar wind/magnetosphere interactions

Keywords: EMIC waves, ULF pulsations, Electron flux dropouts, Dst effect, Magnetopause shadowing, Van Allen Probes

1. Introduction

The Earth's radiation belt environment exhibits a high degree of variability due to both adiabatic and non-adiabatic processes that can swiftly alter particle fluxes. Indeed, many studies have noted that radiation belt electron fluxes can increase, decrease, or even remain the same in response to geomagnetic storms and that this response can appear to be independent of *L* shell or the strength of the storm [e.g. *Reeves et al.*, 2003]. Under the right conditions, the fluxes of outer radiation belt electrons with energies from a few tens of keV up to several MeV can "drop out" or rapidly decrease by one or more orders of magnitude over a broad range of *L* shells due to adiabatic effects and permanent losses to the magnetopause and ionosphere [e.g. *Onsager et al.*, 2002; *Millan and Thorne*, 2007; *Bortnik et al.*, 2006; *Turner et al.*, 2013]. Although electron flux dropouts have typically been associated with the storm main phase, they have also been observed independently of geomagnetic storms [*Morley et al.*, 2010].

70 The "*Dst* effect," in which the development of the storm-time ring current and associated
71 decrease of the inner magnetosphere magnetic field strength causes an observed decrease in the
72 energetic electron fluxes [*Li et al., 1997*, *Kim and Chan*, 1997], is an example of an adiabatic,
73 reversible process that can explain electron flux dropouts. As its name suggests, the key
74 indicator of this effect is a strong correlation between decreases in the energetic electron fluxes
75 and the decrease in the *Dst* index during the storm main phase. Stretching of the magnetic fields
76 due to the formation of a partial ring current near dusk [e.g. *Onsager et al.*, 2002; *Green et al.*,
77 2004] can also produce a localized electron loss due to changes in the magnetic field topology.
78 Since the electron fluxes do not always immediately return to pre-event levels after dropouts,
79 irreversible, non-adiabatic processes causing permanent losses of electrons may also be involved.
80 "Magnetopause shadowing" on the dayside can cause depletions of the electron fluxes when
81 particle drift paths cross the magnetopause and are lost from the magnetosphere [*West et al.*,
82 1972]. Strong, southward interplanetary magnetic fields (IMF) and increases in the solar wind
83 dynamic pressure can cause the last closed drift shell in the dayside magnetosphere to move
84 earthward, resulting in permanent electron losses from the outer regions of the radiation belts
85 [e.g., *Kim et al.*, 2008; 2010; *Matsumura et al.*, 2011; *Yu et al.*, 2013]. Outward radial transport
86 can also contribute to losses to the magnetopause [*Turner et al.*, 2012].
87 Wave-particle interactions with electromagnetic ion cyclotron (EMIC) waves can induce
88 rapid electron scattering [*Thorne and Kennel*, 1971] and may also contribute to permanent losses
89 of relativistic electrons during the storm main phase [*Li et al.*, 1997]. EMIC waves propagate in
90 three bands below the proton gyrofrequency: a hydrogen band between the He^+ and H^+
91 gyrofrequencies, a helium band between the O^+ and He^+ gyrofrequencies, and an oxygen band
92 below the O^+ gyrofrequency. Ion composition and anisotropy [*Kozyra et al.*, 1984; *Thorne and*

93 *Horne*, 1994], along with geomagnetic activity levels [*Bräysy et al.*, 1998] influence which
94 bands are excited. EMIC waves have traditionally been thought of as transverse, left-hand
95 polarized magnetic field fluctuations. However, right-hand and linearly polarized EMIC waves
96 have been observed [*Anderson et al.*, 1992a; *Min et al.*, 2012, *Paulson et al.*, 2014; *Allen et al.*,
97 2015]. Also, some published EMIC wave examples have weak parallel components, and
98 statistical results indicate propagation at large wave normal angles is possible [*Anderson et al.*,
99 1992a; *Anderson et al.*, 1992b; *Min et al.*, 2012; *Allen et al.*, 2015]. EMIC waves affect only
100 relativistic electrons as the resonant energies for wave-particle interactions with these waves are
101 typically above 0.5 MeV [e.g., *Meredith et al.*, 2003].

102 Combinations of adiabatic effects and permanent losses due to magnetopause shadowing
103 and EMIC waves are often responsible for the observed electron behavior. For example, *Bortnik*
104 *et al.* [2006] studied an electron dropout event on 20 November 2003 and found that the behavior
105 of the electrons varied across L shells. For $L > 5$, *Bortnik et al.* [2006] found the dropout was
106 approximately independent of energy, and was consistent with losses to the magnetopause
107 assisted by the *Dst* effect and outward radial diffusion. For $L< 5$, the dropout was energy-
108 dependent and consistent with pitch angle scattering by EMIC waves.

109 In this paper, we present Van Allen Probes, Time History of Events and Macroscale
110 Interactions during Substorms (THEMIS), Geostationary Operational Environmental Satellite
111 (GOES), and Cluster observations during an electron flux dropout that occurred during the 12-14
112 November 2012 geomagnetic storm. We will use the geomagnetic indices and solar wind
113 parameters in the NASA OMNI data set [*King and Papitashvili*, 2005] to examine the upstream
114 drivers of this storm and to determine the sequence of the wave and particle observations in the
115 overall evolution of the storm. During the time period of interest, solar wind flow speeds and

magnetic fields were available from both Wind and the Advanced Composition Explorer (ACE) near L1. However, densities were only available from Wind, so NASA OMNI data for this event are based mainly upon Wind data propagated to the Earth's bow shock nose. Using THEMIS, GOES, and Cluster data, we will discuss the spatial extent of EMIC waves observed on 12-14 November 2012. Electron data from the Van Allen Probes and GOES satellites will be used to examine the development of the flux dropout. We will also examine ULF waves in the Pc4-Pc5 bands observed by the Van Allen Probes and GOES satellites during this event.

2. Start of the Electron Dropout on 12 November Before the Shock Arrival

According to the NOAA Space Weather Prediction Center Preliminary Reports and Forecasts of Solar Geophysical Data issued for 5-11 November 2012 and 12-18 November 2012, the geomagnetic activity on 12-14 November was related to two earthward directed coronal mass ejections (CMEs). The first CME was observed on 9 November at 1524 UT in the Solar and Heliospheric Observatory (SOHO) Large Angle and Spectrometric Coronagraph (LASCO) C2 images [*Brueckner et al.,* 1995] and the second on 10 November in Solar Terrestrial Relations Observatory (STEREO) A COR2 coronagraph images [*Howard et al.*, 2008] at 0504 UT and SOHO/LASCO C3 images at 1054 UT.

Figure 1 shows an overview of the geomagnetic activity and OMNI solar wind parameters at the Earth's bow shock nose, electron data from GOES and the Van Allen Probes, the Dst index, and the Kp index during the 72 hour period starting at 0000 UT on 12 November 2012 and ending at 0000 UT on 15 November 2012. Changes in the solar wind ahead of the shock associated with the CMEs began priming the magnetosphere for development of an electron flux dropout. For the first half of 12 November, the solar wind speed was very low at

both Wind and ACE, with typical values around 280 km/s, and the solar wind B_z GSM was fluctuating around 0 nT. After 1200 UT, the solar wind speed began to increase gradually. A sudden increase in the Wind proton density from ~11 cm^{-3} to 17 cm^{-3} around 1500 UT combined with the increasing solar wind speeds resulted in a jump in the OMNI dynamic pressure from 2 nPa to 4.5 nPa at the bow shock about an hour later at 1600 UT. At about 1800 UT, the B_z GSM component of the interplanetary magnetic field measured by Wind and ACE turned southward ahead of the CME shock.

Figure 2 shows the portions of the GOES, THEMIS A, and Cluster 2 orbits when EMIC waves were observed on 12-13 November as a function of L and magnetic local time. EMIC waves were observed by GOES 14 and 15 for the longest time period of all 5 spacecraft, between 12 November 1610 UT and 13 November 1000 UT. GOES 13, THEMIS, and Cluster observed EMIC waves for shorter intervals within this time period. In order to examine the EMIC waves and ULF pulsations, we transformed the magnetic fields data from these spacecraft into a field-aligned coordinate system commonly used for studying the polarization of low-frequency waves [e.g., *Anderson*, 1994; *Eriksson et al.*, 2005]. We took a 30-minute running magnetic field average to obtain the measured background magnetic field and subtracted this background magnetic field from the total magnetic field to obtain the residual wave magnetic fields. The background magnetic field direction defines the parallel unit vector $\hat{\boldsymbol{p}}$ in our field-aligned coordinate system. The two components perpendicular to the background magnetic field are chosen so

$$\hat{\boldsymbol{e}} = [\hat{\boldsymbol{p}} \times \boldsymbol{R}]/|\hat{\boldsymbol{p}} \times \boldsymbol{R}|$$

where $\boldsymbol{R}$ is the radius vector of the satellite, gives roughly the eastward direction and

$$\hat{\boldsymbol{r}} = \hat{\boldsymbol{e}} \times \hat{\boldsymbol{p}}$$

160 is meridional or radially outward at the magnetic equator. This field-aligned coordinate system
161 can be used to determine the polarizations of ULF pulsations. ULF waves that appear primarily
162 in the spectrograms of the $\hat{\boldsymbol{p}}$ component, which is parallel to the background magnetic field, are
163 compressional. Waves that appear primarily in the radial $\hat{\boldsymbol{r}}$ component are poloidal waves, and
164 waves that appear primarily in the azimuthal or eastward $\hat{\boldsymbol{e}}$ component are toroidal waves [e.g.,
165 *Hughes*, 1994].

166 The top three panels of Figure 3 show spectrograms made by performing a Fast Fourier
167 Transform (FFT) with a sliding Hanning window on the GOES 15 wave magnetic fields in the
168 field-aligned coordinate system described above for the same 72 hour period from 0000 UT on
169 12 November 2012 to 0000 UT on 15 November 2012 shown in Figure 1. The bottom two
170 panels of Figure 3 show the 0.8 and 2.0 MeV electron fluxes and the magnetic field inclination to
171 the orbital plane for GOES 15. Magenta lines for the O^+, He^+, and H^+ ion gyrofrequencies have
172 been overplotted on the spectrograms. Shortly after the increase in solar wind dynamic pressure
173 at the bow shock around 1600 UT, very weak magnetic field fluctuations in the He^+ EMIC wave
174 bands began to be recorded on the dayside at geosynchronous orbit by GOES 15 on 12
175 November around 1610 UT near 7.3 LT, as shown in Figure 3. Figure 4 shows data from the
176 same 72 hour period as Figure 3 for GOES 14, which also began observing very weak
177 fluctuations in the He^+ EMIC band around 1610 UT, near 10.3 LT. This suggests that EMIC
178 waves may have been excited over a broad range of local times on the dayside at
179 geosynchronous orbit by the slight increase in solar wind dynamic pressure near 1600 UT.
180 Figure 5 shows GOES 13 data from the same 72 hour period as Figures 1, 3 and 4. Figure 5
181 shows that GOES 13 began observing intense EMIC waves on 12 November starting at 2121 UT
182 when the satellite was located near 16 LT, and continuing until 2356 UT when the satellite was

183 located near 19 LT. GOES 14 also saw an increase in the intensity of the EMIC waves starting
184 at 2157 UT when the spacecraft had moved to 16 LT that lasted until 0048 UT on 13 November
185 when the spacecraft was located near 19 LT. The increases in the EMIC wave intensity recorded
186 by GOES 13 and GOES 14 on the dusk flank of the magnetosphere were most likely caused by
187 these two satellites moving into a region of stronger wave activity near 16-19 LT.

188 ULF waves in the Pc4 (7-22 mHz) and Pc5 (2-7 mHz) bands [*Jacbos et al.*, 1964] were
189 also observed by the GOES satellites throughout the entire time period shown in Figures 3, 4,
190 and 5, with increased wave amplitudes during intervals of enhanced solar wind drivers. Figure 6
191 shows FFT spectrograms of wave magnetic fields from the Electric and Magnetic Field
192 Instrument Suite and Integrated Science (EMFISIS) [*Kletzing et al.*, 2013] in field aligned
193 coordinates for Van Allen Probe B (RBSP-B) for the same 72 hour time period shown in Figures
194 1, 3, 4, and 5. During the time period of interest, the apogees of the Van Allen Probes were
195 located near dawn. Data from several orbits are shown in Figure 6. Both of the Van Allen
196 Probes observed strong ULF waves throughout the electron dropout and subsequent geomagnetic
197 storm. Compressional Pc4 pulsations were observed by the Van Allen Probes before noon on 12
198 November, as shown by the band near 0.01 Hz in the parallel component of the magnetic field.
199 Lower frequency compressional waves in the Pc 5 frequency range were also observed. Toroidal
200 field line resonances and harmonics were observed in the Pc 4-5 frequency ranges as shown by
201 the eastward component of the magnetic field on 12 November. These are similar to the multi-
202 harmonic toroidal standing Alfvén waves reported in Van Allen Probes data from a few days
203 earlier on 8 November 2012 [*Takahashi et al.*, 2015]. Consistent with *Takahashi et al.* [2015],
204 the toroidal harmonics observed during the time period shown in Figure 6 generally appear to
205 have larger amplitudes when the IMF cone angle shown in Figure 1 is smaller.

206 The bottom panels of Figures 3, 4, and 5 show the 0.8 and 2.0 MeV electron fluxes
207 measured by the EPEAD electron detectors on GOES 13, 14, and 15, as well as the magnetic
208 field inclinations relative to the orbital plane. The standard coordinate system used for GOES
209 magnetic field data is the PEN coordinate system, where the P component is perpendicular to the
210 orbital plane and parallel to the Earth's spin axis, the E component is directed earthward in the
211 orbital plane, and N component is perpendicular to the other two components, pointing eastward.
212 Note that P and E in this coordinate system are not the same as $\hat{\boldsymbol{p}}$ (parallel) and $\hat{\boldsymbol{e}}$ (eastward) in
213 the field-aligned coordinate system. In this coordinate system, the magnetic field inclination
214 angle relative to the orbital plane can be defined as

215 $$\theta = \tan^{-1}\left(\frac{B_P}{\sqrt{{B_E}^2+{B_N}^2}}\right).$$

216 High magnetic field inclinations close to 90° imply a more dipolar magnetic field, while low
217 magnetic field inclinations close to 0° suggest a stretched, tail-like magnetic field. In this paper,
218 the magnetic field inclination is used to determine if the observed electron flux variations are
219 most likely caused by reversible magnetic field changes due to the formation of a partial ring
220 current [e.g. *Onsager et al.*, 2002; *Green et al.*, 2004], as well as the "Dst effect" [*Li et al.*, 1997,
221 Kim and Chan, 1997]. In the radiation belts, the observation of low magnetic field inclinations
222 relative to the orbital plane and tail-like magnetic fields can be interpreted as an indication that
223 the particle trapping boundary may be located earthward of the satellite [e.g. *Onsager et al.*,
224 2002]. However, this does not necessarily mean that the particles have been lost, only that their
225 trajectories have been altered. Note that the decreases in magnetic field configuration associated
226 with the storm-time development of a partial ring current near dusk and the Dst effect, as well as
227 the effects of enhanced solar wind convection on the magnetotail seen on the night side, are

large-scale features that persist for several hours UT and are observed while the GOES spacecraft move through several hours in magnetic local time. On the night side, shorter duration increases in the magnetic field inclination can be superimposed on top of the large-scale decreases in inclination associated with the geomagnetic storm. These shorter duration inclination changes on the night side are likely related to substorm activity and the passage of dipolarization fronts over the spacecraft [e.g. *Sigsbee et al.*, 2005; *Lopez et al.*, 1988]. As the main goal of this paper is to understand the electron behavior over a 72 hour period during a storm in November 2012, we are concerned primarily with changes in magnetic field orientation lasting more than several hours associated with the ring current and convection, and not the short-time scale fluctuations produced by substorm activity. It should be noted that for both the longer time scale magnetic field changes associated with the storm, and the shorter time scale dipolarization fronts, high magnetic inclination angles mean only that the geomagnetic field assumes a more dipole-like configuration, and are not meant to suggest that the field has actually become dipolar.

The 0.8 MeV and 2.0 MeV electron fluxes observed by GOES 13 and GOES 14 were gradually increasing at the start of 12 November 2012. During the time period of increasing electron fluxes on 12 November, the magnetic fields at GOES 13 and 14 were highly dipolar. The 2 MeV electron flux measured reached its maximum value at GOES 14 at 1709 UT and at GOES 13 a few minutes later at 1713 UT on 12 November. The 2 MeV electron flux observed by GOES 13 began to decrease after reaching its peak value at 1713 UT, so that it had already reached instrumental background levels by 2201 UT, more than an hour before the shock arrival and sudden impulse at 2316 UT. The 2 MeV electron flux at GOES 14 also began to decrease

250 after its peak value at 1709 UT, until it reached instrumental background levels at 2230 UT, also
251 well before the shock arrival.

252 The GOES 13 and GOES 14 0.8 MeV electron fluxes reached their peak values on 12
253 November at 1713 UT, simultaneously with the 2 MeV electrons at GOES 13. After reaching
254 peak values on 12 November, the 0.8 MeV electron fluxes observed by all three GOES
255 spacecraft began to decrease throughout the rest of the day, but did not reach their minimum
256 values until after the shock arrival on 13 November. At first, the 0.8 MeV electron fluxes at
257 GOES 13 and 14 decreased gradually. However, when the magnetic field at these two satellites
258 started to become more stretched, the 0.8 MeV electron fluxes began to decrease rapidly. The
259 magnetic field inclination at GOES 13 was consistently above 70° degrees until 2154 UT on 12
260 November, when GOES 13 was located near 16.9 LT. After this time the magnetic field
261 inclination began to decrease over the next 4 hours, dropping to about 17° by 0100 UT on 13
262 November, when GOES 13 was located at 20 LT. At GOES 14, the magnetic field inclination
263 remained consistently above 60°-70° until about 2200 UT on 12 November, when GOES 14 was
264 located near 16.4 LT. After this time, the magnetic field inclination at GOES 14 dropped steeply
265 until 0105 UT on 13 November, when GOES 14 was located near 19.2 LT. The highly
266 stretched magnetic fields observed by GOES 13 and 14 near dusk are likely related to
267 development of a partial ring current.

268 The behavior of the magnetic fields and electron fluxes at GOES 13 and 14 was similar,
269 most likely due to the proximity of these two satellites in local time. The changes in the
270 magnetic configuration and timing of the electron flux decreases were different at GOES 15,
271 which is separated from GOES 13 and 14 by a few hours in local time, and is located about 5°
272 lower in magnetic latitude than GOES 13 and 14. As at GOES 13 and 14, the 0.8 MeV and 2.0

MeV electron fluxes observed by GOES 15 gradually increased from the start of 12 November 2012. However, the 2 MeV electron flux observed by GOES 15 did not reach its maximum value on 12 November until very late in the day at 2054 UT. The magnetic field inclination at GOES 15 was close to 75° from 0000 UT on 12 November up to the time of the shock arrival at 2316 UT on 12 November. This is rather interesting as GOES 15 was located on the dayside near 15 LT at 0000 UT, passed through midnight at 0833 UT, and reached 6 LT at 1442 UT, indicating that GOES 15 observed somewhat dipolar fields all across the night side on 12 November. The 2 MeV electron flux at GOES 15 decreased after reaching its peak value on 12 November, but did not reach instrumental background levels until after the start of 13 November. The 0.8 MeV electron flux did not reach its peak value at GOES 15 until 1950 UT on 12 November, much later than at GOES 13 and 14. The 0.8 MeV electron flux peak at GOES 15 occurred about an hour before the 2.0 MeV peak, unlike at GOES 13 and 14 where the 0.8 and 2.0 MeV fluxes peaked around the same time. After reaching peak values on 12 November, the 0.8 MeV electron fluxes observed by GOES 15 decreased throughout the rest of the day, but did not reach their minimum values until after the shock arrival on 13 November.

The initial development of the electron dropout on 12 November appears reasonably well-correlated with the development of stretched magnetic fields near dusk and the start of EMIC waves at geosynchronous orbit. The two satellites closest to dusk, GOES 13 and 14, observed the start of the electron dropout first, while GOES 15, which was located at earlier local times observed the start of the dropout after GOES 13 and 14. The relative timing of the start of the electron dropout at GOES 13, 14, and 15 is likely related to the observed differences in the local magnetic field configurations near noon and on the dusk flank and the drifts of the electrons through these different fields.

3. Shock Arrival and Continuation of the Electron Dropout on 13 November 2012

The shock associated with the CMEs arrived at ACE on 12 November 2216 UT, and was followed by the observation of a 16 nT sudden impulse by the Boulder USGS magnetometer an hour later at 2316 UT. The maximum southward IMF B_z reached was -19.5 nT at 2338 UT and the total IMF reached a maximum value of 22.8 nT on 13 November at 0053 UT. The solar wind speed measured by ACE peaked at 504 km/s at 0111 UT on 13 November. Geomagnetic activity levels were unsettled to active throughout 13 November due to the shock arrival, as indicated by the increase in the Kp index. EMIC waves continued to be observed by GOES 13, 14, and 15 after the shock arrival and were also observed by Cluster and THEMIS on 13 November. The Van Allen Probes observed bursty, broadband ULF waves around the time of the shock arrival that crossed all three EMIC wave bands. Strong ULF fluctuations in the Pc4-5 frequency ranges and above were observed throughout the rest of the 13 November. Sometimes these waves had harmonic structures that appeared consistent with ULF field line resonances.

A sudden increase in the intensity of the EMIC waves observed by GOES 15 near 14 LT was associated with the arrival of the shock at 2316 UT on 12 November. The strong wave activity observed by GOES 15 continued until about 0340 UT on 13 November, when GOES 15 was located near 18.5 LT. Before the shock arrival, the EMIC waves in the He^+ band at GOES 15 appeared most strongly in the parallel component of the magnetic field, with small bursts in the eastward and radial components. After the shock arrival, the EMIC waves at GOES 15 were most intense in the eastward component of the magnetic field. O^+ band waves may also have been observed, but they are difficult to separate from the strong ULF waves in the Pc4-5 bands that were also observed around the time of the shock arrival.

319 Although the shock arrival excited very strong EMIC waves on the dayside at GOES 15
320 near 14 LT, it only had a modest effect on the EMIC waves observed further down the flanks of
321 the magnetosphere by GOES 14 and GOES 13. A burst of slightly more intense EMIC waves
322 was observed by GOES 14 near 17 LT around 2316 on 12 November and appears to be related to
323 the shock arrival. As at GOES 15, the strongest fluctuations in the He^+ band at GOES 14
324 switched from the mainly the parallel component before the shock arrival to the eastward
325 component of the magnetic field after the shock arrival. Only a very slight increase in the EMIC
326 wave intensity was observed by GOES 13 near 18 LT around the time of the shock arrival.
327 Strong ULF waves in the Pc4-5 frequency range were also observed by GOES 13 and 14.
328 Some of the ULF wave power observed by the Van Allen Probes in Figure 6 extended
329 upwards into the He^+ and H^+ EMIC wave frequency ranges at the time of the shock arrival and
330 solar sector boundary crossing. However, much of the ULF wave power recorded by the Van
331 Allen Probes throughout this event was due to waves at frequencies well below 1/10 of the O^+
332 cyclotron frequency. The character of the waves observed by the Van Allen Probes was not
333 consistent with EMIC waves, as some wave bursts extended across all three EMIC wave bands
334 and above the H^+ cyclotron frequency. The apogee of the Van Allen Probes was located near
335 dawn, so it is not surprising that EMIC waves were not observed by the Van Allen Probes as
336 statistical studies generally show that EMIC waves are observed most often near dusk [*Anderson*
337 *et al.*, 1992a; 1992b]. It appears that EMIC waves were mainly observed outside the orbits of the
338 Van Allen Probes during this event, consistent with studies that show the occurrence rate of
339 EMIC waves is low inside of geosynchronous orbit [*Usanova et al.*, 2012] and that dawn side
340 EMIC waves tend to have smaller amplitudes and occur at larger radial distances than on the
341 dusk side [*Min et al.*, 2012]. Toroidal Pc 4-5 field line resonances and harmonics continued to

342 be observed in the eastward component of the magnetic field by the Van Allen Probes on 13
343 November

344 Figure 7 shows the THEMIS-A FGL [*Angelopoulos*, 2008; *Auster et al.*, 2008] magnetic
345 field in field-aligned coordinates shortly after the shock arrival, from 0005 to 0230 UT on 13
346 November 2012. Only THEMIS slow survey data at 3 second resolution were available before
347 13 November 0000 UT, which do not have sufficient time resolution for studying He^+ and H^+
348 EMIC waves in this region. He^+ band EMIC waves are clearly seen in the THEMIS data, along
349 with possible H^+ band waves. Lower frequency O^+ band waves may also be present, but are
350 difficult to separate from the strong ULF waves observed throughout the time period shown.
351 The fluctuations observed by THEMIS-A are strongest in the perpendicular wave magnetic field
352 components, but also have a weaker parallel component. THEMIS-A observed these EMIC
353 waves at radial distances between 6.3 and 9.1 R_E from 13.3 to 14.5 LT. The EMIC waves
354 observed by THEMIS-A continue all the way out to the magnetopause on the dayside. The
355 location of the THEMIS-A EMIC wave observations in the afternoon sector suggests the
356 presence of a plasmaspheric plume, as EMIC waves have been associated with drainage plumes
357 in the afternoon sector by past studies [*Morley et al.*, 2009; *Fraser et al.*, 2010; *Halford et al.*,
358 2015; *Yuan et al.*, 2010; *Yuan et al.*, 2013]. These waves may be generated by enhanced cold
359 plasma densities within the plume [*Morley et al.*, 2009; *Halford et al.*, 2015]. Several hours of
360 southward IMF occurred before the CME arrival and the observation of the EMIC waves by
361 THEMIS-A, which is also consistent with the presence of a plume, as they are more likely to
362 occur when convection is enhanced [e.g., *Walsh et al.*, 2013]. According to statistical analysis of
363 THEMIS data presented by *Walsh et al.* [2013], the most common location where plumes contact
364 the magnetopause is at 13.6 MLT. This is also consistent with the location of THEMIS-A during

365 the event we studied.

366 After the main intervals of intense EMIC waves observed on 12-13 November by GOES
367 13 and 14 near dusk and by GOES 15 around the time of the sudden impulse, bursty waves in the
368 EMIC frequency bands were recorded by all three GOES satellites and Cluster 2. Later in the
369 day on 13 November, another short burst of EMIC waves was observed by GOES 14 from 0239
370 UT to 0305 UT between 20.7 and 21.2 LT, and GOES 13 between 21.3 to 21.8 LT, possibly due
371 to a sudden spike in the solar wind dynamic pressure near this time. Another burst of EMIC
372 wave activity was observed between 13 November 0550 UT to 0715 UT by GOES 15 (21 LT)
373 and GOES 14 (near 0.7 LT). Figure 8 shows EMIC waves observed by Cluster 2 FGM [*Balogh*
374 *et al.*, 2001] on 13 November between 0615 and 0640 UT near 17 LT. Note that in Figure 8, the
375 Cluster spin period (4 seconds) is visible as a very narrow, flat line across the entire plot at 0.25
376 Hz. The bursty EMIC wave activity recorded by GOES 14, GOES 15, and Cluster 2 between
377 0550 UT and 0715 UT may have been associated with solar wind dynamic pressure fluctuations
378 around this time, but there are no clear correlations between specific wave bursts and pressure
379 variations.

380 To verify the identification of EMIC waves and to better understand the evolution of the
381 EMIC wave properties before and after the shock arrival, the GOES 15 wave magnetic fields
382 were analyzed with the PRopagation Analysis of STAFF-SA Data with COherency tests
383 (PRASSADCO) software. PRASSADCO implements analysis methods to estimate the sense of
384 polarization, ellipticity, and wave vector direction described respectively by *Santolík et al.*
385 [2001; 2002; 2003]. Because the GOES satellites do not have electric field data, we cannot
386 determine Poynting vectors or resolve waves propagating anti-parallel to one another as their
387 magnetic fields will appear to be the same, but neither is important for wave identification. At

388 frequencies below the proton cyclotron frequency, there are three possible wave modes: EMIC
389 waves, magnetosonic waves, and Alfvén waves [*Gurnett and Bhattacharjee*, 2005]. Both Alfvén
390 waves and magnetosonic waves are typically linearly polarized, but EMIC waves are normally
391 left-hand polarized. There are reports in the literature (as discussed earlier) of linear and right-
392 hand polarizations for EMIC waves, but those are not typical. Results from the analysis of 30
393 hours of GOES 15 data from 1200 UT on 12 November to 1800 UT on 13 November with
394 PRASSADCO are shown in Figure 9. As the PRASSADCO analysis assumes plane waves, the
395 results can be poorly determined when the planarity is low. The ellipticity, wave normal angle,
396 and planarity are therefore only plotted in Figure 9 when the wave power in the total magnetic
397 field is greater than
398 10^{-2} nT^2/Hz, and the planarity is greater than 0.5. These thresholds were used to analyze the
399 most intense EMIC waves and ensure that Figure 9 only shows the ellipticity and wave normal
400 angle when the PRASSADCO results are well-determined. The ion cyclotron frequencies have
401 been overplotted in Figure 9 with magenta lines on the spectrograms of the total magnetic field
402 power, the ellipticity (-1 is left-handed, 0 is linear, and +1 is right-handed), and wave normal
403 angle, and in turquoise on the planarity. These colors were chosen for the frequencies to make
404 them stand out from narrow instrumental lines due to the spacecraft heater that appear between
405 0.3 to 0.4 Hz and near 0.2 Hz. As can be seen in Figure 9, the He^+ EMIC band waves observed
406 by GOES 15 on 12 November from 1600 UT up to the shock arrival at 2316 UT were mainly
407 left-handed (as indicated by the blue color) with large wave normal angles, greater than 70°.
408 However, the bursts of He^+ EMIC waves appearing in the eastward and radial components of the
409 GOES 15 magnetic field between 1800 and 2000 UT were clearly left-hand polarized and had
410 wave normal angles less than 30°, consistent with parallel propagation. The weak fluctuations in

411 the H^+ EMIC band observed from around 2000 UT to 2316 UT were mostly left-hand polarized
412 with some linearly polarized waves and large wave normal angles. These H^+ band waves do not
413 appear in the wave normal analysis shown Figure 9 because they were below the 10^{-2} nT^2/Hz
414 amplitude threshold chosen for this figure. GOES 15 was located between 7.3 LT and 14.3 LT
415 when the nearly perpendicular propagating, left-hand to linearly polarized EMIC waves were
416 observed, which is consistent with statistical studies showing that dawn side waves tend to be
417 more linearly polarized and have large wave normal angles in the H^+ band (>45°) and even larger
418 wave normal angles in the He^+ band (>60°) [e.g., *Anderson et al.*, 1992; *Min et al.*, 2012; *Allen et*
419 *al.*, 2015].

420 The wave normal angle of the He^+ and H^+ band EMIC waves observed by GOES15
421 abruptly drop to less than 20° when the CME shock arrives at 2316 UT on 12 November,
422 indicating parallel propagation. The He^+ band waves now appear to be strongly left-hand
423 polarized, while the H^+ band is left-hand to slightly linearly polarized. These conditions persist
424 between 2316 UT on 12 November to 0600 UT on 13 November, when GOES 15 was located
425 between 14.3 LT and 21.4 LT. This is consistent with statistical studies showing that dusk side
426 EMIC waves tend to be left-hand to linearly polarized and have smaller wave normal angles
427 [*Anderson et al.*, 1992; *Min et al.*, 2012]. Around 0600 UT on 13 November, the wave normal
428 angles in both the He^+ and H^+ bands abruptly increase to values greater than 70° again,
429 indicating perpendicular propagation. The polarizations after 0600 UT are mainly linear, with
430 some left-hand polarized waves. Although the behavior of the EMIC waves during this event is
431 similar to documented local time effects on EMIC wave properties, upstream solar wind
432 conditions associated with the CME arrival also appear to have had an effect. Before the CME
433 arrival, the IMF cone angle in Figure 1 was generally greater than 100°. From 2316 UT on 12

November to 0600 UT on 13 November, the IMF cone angle fluctuated, typically between values of 50° to 80°. After 0600 UT on 13 November, the IMF cone angle was consistently greater than 100° again. The intervals where the EMIC waves had nearly perpendicular propagation seem to roughly coincide with the intervals of higher IMF cone angles, while the parallel propagating waves occurred during lower IMF cone angles. EMIC waves observed in space tend to be very bursty and localized, similar to the short burst of waves observed by Cluster during this event shown in Figure 8. One of the most unique features of the EMIC waves observed by GOES 15 on 12-13 November was the extended duration of these waves over several hours UT and the broad range of magnetic local times on the day side over which they were observed, as shown by Figures 2, 3, and 9.

The relativistic electron populations continued to evolve throughout 12-13 November in response to the ongoing EMIC wave activity, the arrival of the interplanetary shock, and further changes in the magnetic field configuration of the inner magnetosphere. The 2 MeV electron flux at GOES 13 and 14 remained flat at instrumental background levels, but the 2 MeV electron flux at GOES 15 continued decreasing from its peak value at 2054 UT on 12 November until 0103 UT on 13 November when it finally dropped to instrumental background levels. By the time of the sudden impulse at 2316 UT, the GOES 13 0.8 MeV electron flux had already dropped to less than 3% of its peak value at 1713 UT on 12 November and it continued to decrease, reaching a minimum value at 13 November 0239 UT. By the time of the sudden impulse at 2316 UT, the GOES 14 0.8 MeV electron flux, which had also peaked at 1713 UT on 12 November, had dropped to about 5% of its maximum value. The GOES 14 0.8 MeV electron flux reached its minimum value at 13 November 0241 UT, just 3 minutes later than GOES 13. At the time of the sudden impulse, the GOES 15 0.8 MeV electron flux had dropped only to 58%

457 of its peak value on 12 November at 1950 UT, but it continued to decrease for several more
458 hours on 13 November.

459 The Van Allen Probes provided information about both the spatial and temporal
460 evolution of the electron fluxes [*Baker et al.*, 2012; *Blake et al.*, 2013] near the time of the shock
461 arrival. Figure 10 shows the energetic electron fluxes observed by Van Allen Probe B (RBSP-B)
462 for energies of 134 keV, 235 keV, 459 keV, 875 keV, 1040 keV and 2 MeV as a function of time
463 and L shell for the 72 hour period from 0000 UT on 12 November to 0000 UT on 15 November.
464 The 875 keV channel was selected because it was the closest in energy to the 0.8 MeV electrons
465 measured by the GOES satellites. The electron data from Van Allen Probe A (RBSP-A) are
466 similar to those shown in Figure 10. The electron flux dropout was first observed by the Van
467 Allen Probes in the dawn magnetosphere after both spacecraft exited the plasmasphere and
468 moved towards higher L shells around the time of the shock arrival.

469 Because Figure 10 shows that the electron flux dropout was more pronounced on the
470 higher L shell portions of the Van Allen Probes orbits, we compared the electron fluxes with the
471 location of the plasmapause to confirm that the apparent losses were not just due to the
472 spacecraft leaving the plasmasphere. During the orbit (199 for RBSP-A, 198 for RBSP-B) just
473 before the shock arrival on 12 November, the electron fluxes for energies close to 0.8 MeV and
474 2.0 MeV at both of the Van Allen Probes were well above instrumental background levels as the
475 spacecraft reached apogee in the dawn magnetosphere. On the next orbit (200 for RBSP-A, 199
476 for RBSP-B), electron densities obtained from the upper hybrid line in the EMFISIS plasma
477 wave [*Kurth et al.*, 2015] data undergo a steep drop when both spacecraft crossed a sharp
478 plasmapause boundary. RBSP-A observed the electron density drop by a factor of 130 between
479 2155 UT on 12 November when the spacecraft was located at L=4.2 and 2.9 LT and 2221 UT

480 when the spacecraft was located at L=4.8 and 3.5 LT, just outside the plasmapause. For RBSP-
481 B, the electron density dropped by a factor of 90 between 2219 UT on 12 November when the
482 spacecraft was located at L=4.0 and 2.8 LT and 2259 UT when the spacecraft left the
483 plasmasphere at L=4.9 and 3.6 LT. The Van Allen Probes density measurements suggest that
484 the plasmapause was located between about L=4-5 in the local time region between 3.0 to 3.5 LT
485 during this outbound crossing. The minimum density was measured by RBSP-A on this orbit at
486 2320 UT on 12 November when RBSP-A was located at L=5.8 and 4.4 LT. The minimum
487 density was measured by RBSP-B at 0054 UT on 13 November at L=6.2 and 5.1 LT.

488 In the energy channel closest to 0.8 MeV measured by RBSP-A, a steep drop in the
489 electron flux started at 2314 UT when the spacecraft was located at L=5.7 and 4.3 LT. RBSP-B
490 observed a steep drop in the 0.8 MeV electron flux starting at 2315 UT when the spacecraft was
491 located at L=5.2 and 3.8 LT. The 2.0 MeV electron flux observed by both RBSP-A and RBSP-B
492 also began to drop rapidly to instrumental background levels at this time. According to the
493 electron densities both RBSP-A and RBSP-B were already located outside the plasmapause
494 when the electron fluxes began to decrease, indicating that the flux decreases observed by the
495 Van Allen Probes for L > 5 in the dawn side magnetosphere were related to the shock arrival and
496 were not simply due to the spacecraft exiting the plasmasphere.

497 As shown in Figure 10, a decrease in the Van Allen Probes electron fluxes was observed
498 from 134 keV up to 2.0 MeV at the time of the shock arrival. Figure 10 shows that over the next
499 few orbits, the 134 keV electron fluxes from L~ 4 to 6 actually increased dramatically to levels
500 greater than their values before the CME arrival and the 235 keV and 459 keV electrons quickly
501 recovered from the decrease seen at the CME arrival. The 875 keV, 1040 keV, and 2.0 MeV
502 electrons shown in Figure 10 increased slightly on the orbit after the CME arrival, but they

503 remained at lower levels than before the CME arrival over the next several orbits, for a period of
504 time similar to the dropout in the 2 MeV electrons observed by GOES. The recovery of the
505 lower energy electrons suggests that adiabatic processes may have played a role during this
506 event, while the prolonged dropout in the higher energy electrons suggests non-adiabatic
507 processes also resulted in a permanent loss of some of the electron population.

508 The magnetic fields at GOES 13 and 14 remained stretched for several hours after the
509 sudden impulse. The magnetic field inclination at GOES 13 began to rise after 0500 UT on 13
510 November, reaching a value of about 60° by 0650 UT, when GOES 13 was located at 2.2 LT.
511 The GOES 14 inclination angle began to increase after the satellite passed through local
512 midnight around 0540 UT on 13 November, reaching values above 60° around 0700 UT on 13
513 November when GOES 14 was located near 1.5 LT. While the stretched fields observed near
514 dusk by GOES 13 and 14 may be due to formation of a partial ring current, enhanced solar wind
515 convection probably contributed to the stretched fields observed by GOES 13 and 14 across the
516 night side. Although the magnetic field inclinations at GOES 13 and 14 had returned to more
517 dipolar configurations by 0700 UT on 13 November, the 2 MeV electron fluxes at all three
518 geosynchronous satellites remained at instrumental background levels. The 0.8 MeV electron
519 fluxes begin increasing slowly after GOES 13 and 14 began observing more dipolar fields, but
520 continued to remain well below the peak fluxes observed on 12 November.

521 At the time of the shock arrival GOES 15 was located close to noon at 13.3 LT and the
522 magnetic field inclination actually increased slightly, from about 75° to 85° due to compression
523 of the magnetosphere by the shock. The magnetic field inclination at GOES 15 remained above
524 70° until 0426 UT on 13 November, when GOES 15 was located near dusk at 19.7 LT and the
525 magnetic field inclination started to decrease rapidly. The GOES 15 magnetic field inclination

526 dropped to about 52° at 0522 UT when the satellite was located near 20.6 LT. At around 0600
527 UT, near 21.4 LT, the magnetic field inclination at GOES 15 jumped quickly to values above
528 70°, indicating possible propagation of a substorm dipolarization front past the spacecraft. After
529 the dipolarization front passed, the magnetic field at GOES 15 became more tail-like again and
530 the inclination briefly dropped to about 40° at 0640 UT when the satellite was located near 22.1
531 LT. After about 0715 UT on 13 November, when GOES 15 was located near 22.7 LT, the
532 GOES 15 inclination remained consistently above 60° throughout the rest of the day. Even
533 though GOES 15 did not observe the extreme changes in magnetic field inclination that GOES
534 13 and 14 did, the 0.8 and 2.0 MeV fluxes at GOES 15 behaved in a similar manner to those at
535 GOES 13 and 14.

536 The highly stretched magnetic fields observed by GOES 13 and 14 on 12-13 November
537 suggest that the electron dropout was partially due to adiabatic effects. However, the behavior of
538 the 0.8 MeV electrons at GOES 15 is similar to their behavior at GOES 13 and 14, even though
539 GOES 15 never encounters the strongly tail-like magnetic fields observed by GOES 13 and 14.
540 In spite of ongoing changes in the magnetic field configuration at geosynchronous orbit on 13
541 November, the 2 MeV electron fluxes at geosynchronous orbit remained at instrumental
542 background levels until 14 November. The electron fluxes for the highest energies observed at
543 the Van Allen Probes also remained at reduced levels throughout 13 November. This implies
544 that in addition to adiabatic effects, there was also a permanent loss of electrons, likely due to the
545 effects of the EMIC waves observed by GOES, THEMIS and Cluster, or losses to the
546 magnetopause.

547

548 **4. Solar Sector Boundary Crossing and the 13-14 November 2012 Electron Dropout**

549 Throughout 13-14 November 2012, the solar wind speed remained elevated.
550 Geomagnetic activity increased to major storm levels early on 14 November due to a prolonged
551 period of negative IMF B_z related to the CMEs and a solar sector boundary crossing which
552 reached Earth's bow shock on 14 November at 0336 UT. The solar sector boundary crossing
553 was followed by a negative polarity coronal hole high speed stream. Eventually, a storm
554 developed with minimum Dst of about -100 nT at 0700 UT on 14 November.

555 The 2.0 MeV electron fluxes at GOES 13, 14, and 15 continued to remain at instrumental
556 background levels throughout 13 November, even though the 0.8 MeV fluxes had recovered
557 slightly by the end of the day. The 0.8 MeV flux reached peak values at GOES 13 at 2320 UT,
558 GOES 14 at 2301 UT, and GOES 15 at 2258 UT. During the time period when the 0.8 MeV
559 fluxes were recovering the magnetic field inclinations at GOES 13, 14 and 15 indicated that the
560 satellites were in a region of highly dipolar fields. The recovery of the 0.8 MeV electron fluxes
561 was likely related to a combination of the magnetic field configuration changes and acceleration
562 by chorus and ULF waves which began to be observed by the Van Allen Probes after the shock
563 arrival.

564 After the brief recovery, a second dropout in the 0.8 MeV electron fluxes at
565 geosynchronous orbit occurred on 14 November as the geomagnetic storm developed and Dst
566 decreased. The 134 keV, 235 keV, and 459 keV, 875 keV, and 1040 keV electron fluxes on
567 RBSP-B in Figure 10 also show another slight decrease around this time. At geosynchronous
568 orbit, the development of this dropout appeared to be strongly correlated with the Dst index, as
569 shown by Figure 1, and with the magnetic field inclinations as shown by Figures 3, 4, and 5. As
570 on 12-13 November, the 0.8 MeV flux decrease was also strongly correlated with the observation
571 of stretched magnetic fields from dusk to dawn. During the 14 November dropout, the 0.8 MeV

572 electron fluxes had a greater level of fluctuations than during the 13 November dropout. Brief
573 fluctuations in the magnetic field inclination up to near 40° at GOES 14 on the night side
574 between 0045 and 0825 UT on 14 November may indicate a series of dipolarization fronts
575 associated with substorm activity in the magnetotail. Similar fluctuations were observed by both
576 GOES 14 and 15. The variations in the 0.8 MeV electron fluxes often appeared to be correlated
577 with these fluctuations in the magnetic field inclination. After the passage of each dipolarization
578 front, the magnetic field returned to a highly stretched configuration and the 0.8 MeV fluxes
579 decreased again. As shown in Figure 1, the Kp index increased at the beginning of 14
580 November, possibly in response to the southward IMF. Kp remained elevated until noon, which
581 appears consistent with the observation of substorm activity during the main phase of the storm.
582 The return of the electron fluxes to pre-storm levels finally started as the Dst index began
583 to increase and the magnetic field inclinations at geosynchronous orbit began increasing to a
584 more dipolar configuration around 0900 UT. The change in magnetic field configuration was
585 accompanied by increases in the 0.8 MeV and 2 MeV electron fluxes. The 0.8 MeV electron
586 fluxes returned to their pre-storm levels at GOES 13 at 1323 UT on 14 November, and reached
587 their maximum value for the day at 1548 UT. The GOES 13 2.0 MeV electron flux returned to
588 its pre-storm level several minutes later at 1338 UT on 14 November, and continued to increase
589 until reaching its maximum value for the day at 1548 UT, simultaneously with the 0.8 MeV
590 electrons. For GOES 14, the return to the pre-storm 0.8 MeV flux levels occurred at 1329 UT
591 and the maximum value was reached at 1715 UT. The 2.0 MeV electron flux at GOES 14
592 returned to its pre-storm value at 1344 UT on 14 November and reached its maximum value for
593 the day at 1659 UT. At GOES 15, the 0.8 MeV fluxes returned to their pre-storm value at 1332
594 UT and reached their peak value at 2116 UT. At GOES 15, the 2.0 MeV electron flux reached

its pre-storm value at 1350 UT on 14 November and reached its maximum value near the end of the day at 2115 UT.

On 14 November, bursty, low-frequency waves were observed by all three GOES satellites and the Van Allen Probes in association with an increase in the solar wind dynamic pressure at the beginning of the day, a few hours before the solar sector boundary crossing. These waves were broadband and did not feature the clear EMIC band structures that the waves observed by the GOES satellites on 12-13 November had. Analysis of the GOES 15 data with PRASSADCO shows the waves observed on 14 November had mixed polarizations, but were mainly linearly to right-hand polarized, with a very wide range of propagation directions. The absence of clear frequency bands and the PRASSADCO results suggest these broadband ULF waves are not likely to be EMIC waves. The wave bursts observed by the Van Allen Probes were also broadband and extended across all three EMIC frequency bands to above the H^+ cyclotron frequency. As on 12 and 13 November, the ULF wave activity observed by the Van Allen Probes on 14 November did not appear to be consistent with EMIC waves because the most intense wave power was concentrated well below 1/10 of the O^+ cyclotron frequency and was within the Pc 4-5 frequency ranges. Harmonic structures typical of field line resonances can also be seen eastward component of the Van Allen Probes magnetic field on 14 November. Just before the end of 14 November, all three GOES satellites observed a strong Pc 4-5 pulsation. This pulsation appeared in all three components of the magnetic field, but it was strongest in the parallel and radial components of the magnetic field, suggesting mainly compressional and poloidal pulsations. Compressional Pc 5 pulsations are typically associated with storms and subtorms [*Barfield and McPherron*, 1978; *Anderson*, 1994], while poloidal Pc 4-5 pulsations are often observed during the recovery from prior geomagnetic activity [*Takahashi et al.*, 1990;

618 *Eriksson et al.*, 2005; 2008; *Liu et al.*, 2009] and are associated with plasmaspheric refilling
619 [*Engebretson et al.*, 1992]. Although these ULF waves do not appear to be associated with the
620 electron losses, they likely contributed to the recovery of the energetic electrons at the end of the
621 storm.
622
623 **5. Discussion**
624 The development of the initial electron flux dropout on 12-13 November at
625 geosynchronous orbit occurred over time periods equivalent to many electron drift orbits.
626 Although start time of the electron flux dropout varied between spacecraft, the number of drift
627 periods it took for the fluxes to reach their minimum value at both energies were similar at all
628 three GOES spacecraft. For 2 MeV electrons, the bounce-averaged drift in a dipolar magnetic
629 field [*Parks*, 1991] is about 5 minutes, and for 0.8 MeV electrons it is about 12 minutes. The 2
630 MeV electron flux at GOES 13 took 288 minutes or 58 drift periods to drop from the peak on 12
631 November at 1713 UT to below detectable levels. At GOES 14 it took 321 minutes (67 drift
632 periods), and at GOES 15 it took 249 minutes (50 drift periods) to drop from the peak value at 12
633 November 2054 UT to its lowest point at 13 November 0103 UT. Although the 2 MeV flux at
634 GOES 15 did not peak until nearly 3.75 hours later than the 2 MeV flux at GOES 13 and 14, the
635 number of drift periods for the electron fluxes at this energy to reach instrumental background
636 levels at GOES 15 was similar to that at GOES 13 (60 drift periods) and GOES 14 (67 drift
637 periods). For the 0.8 MeV electrons it took 566 minutes or about 47 drift periods from the peak
638 in the GOES 13 electron at 12 November 1713 UT to reach the minimum flux value at 13
639 November 0239 UT. At GOES 15, the 0.8 MeV electron flux took 818 minutes, or about 68 drift
640 periods to reach its minimum value on 13 November at 0928 UT.

641 It is fairly typical for the development of electron dropout events to depend upon energy
642 and local time [*Onsager et al.*, 2002; *Green et al.*, 2004]. In a study of 52 electron dropout
643 events with rapid decreases in the >2 MeV electron fluxes at geosynchronous orbit, the events
644 typically began in the dusk sector, simultaneously with the stretching of the magnetic field
645 caused by the formation of a partial ring current driven by upstream solar wind conditions
646 [*Green et al.*, 2004]. As the discussion in the previous paragraph indicates, the event studied
647 here follows this pattern, because GOES 13, which was located the closest to dusk on 12
648 November, observed the start of the electron flux dropout well before GOES 15, which was
649 located the furthest away from dusk of the three geosynchronous satellites at the start of the
650 dropout. The Van Allen Probes, which had apogee near dawn around the time of the shock
651 arrival on 12 November, were the last to observe the dropout. It is also interesting to note that
652 during the start of the first interval of reduced 0.8 MeV electron fluxes on 12-13 November, the
653 degree of stretching indicated by the magnetic field inclination at GOES 15 was much less than
654 that at GOES 13 and 14. However, all three geosynchronous satellites observed a similar degree
655 of stretching on 14 November during the second interval of decreased 0.8 MeV electron fluxes.
656 GOES 15 was near similar local times at the start of both intervals of reduced 0.8 MeV electron
657 fluxes. The differences in the responses of the magnetic field and electrons at GOES 15 may be
658 due to both the differences in the solar wind drivers and state of the magnetosphere during these
659 two time periods.

660 As shown by Figure 1, 3, 4, and 5, the initial phase of the electron flux dropout on 12-13
661 November does not appear to be the result of the Dst effect. There could be a correlation
662 between the decrease in the 2 MeV electron fluxes at GOES 13 and 14 at the start of the dropout
663 on 12 November and a slight decrease in the Dst index around the same time, but no correlation

664 is seen with the 2 MeV electrons at GOES 15. The 2 MeV electrons at all three GOES satellites
665 quickly reached instrumental background levels on 12-13 November and remain at that level
666 until Dst begins to recover near the end of the day on 14 November. The behavior of the 0.8
667 MeV electrons at GOES 13, 14, and 15 also does not appear to track the Dst index throughout 12
668 November and most of 13 November, and instead appears to be better correlated with stretching
669 of the magnetic field. In the early afternoon on 13 November, the GOES 13, 14, and 15 0.8
670 MeV electron fluxes actually begin to recover, while the Dst index has a gradual decreasing
671 trend. However, the second phase of the 0.8 MeV electron flux decrease, which starts at the end
672 of 13 November definitely follows the Dst index as it drops steadily to values below -100 nT on
673 14 November. Both the 0.8 MeV and 2 MeV electron fluxes at all three GOES satellites begin to
674 recover as Dst increases, but the 2 MeV electron fluxes take longer to increase. This may be
675 because the dropout in the 0.8 MeV electrons on 13-14 November was caused mainly by
676 adiabatic processes, so that the electrons recovered quickly in response to magnetic field
677 configuration changes at the end of the storm. The prolonged decrease in the 2 MeV fluxes from
678 12-14 November appears to have represented a permanent loss of electrons, and thus the 2 MeV
679 fluxes required the acceleration of lower energy electrons to fully recover.

680 Although the GOES satellites did not observe any magnetopause crossings at
681 geosynchronous orbit during this event, there were strong variations in the solar wind dynamic
682 pressure and intervals of southward IMF during the time period of interest. Such variations in
683 upstream conditions have been associated with permanent losses to the magnetopause by recent
684 studies [e.g., *Kim et al.*, 2008; 2010; *Matsumura et al.*, 2011; *Yu et al.*, 2013]. As noted by
685 *Matsumura et al.* [2013], if geosynchronous satellites are the furthest satellites from Earth used
686 in a study, the outermost edge of the radiation belt associated with electron losses to the

687 magnetopause might not be detected. As a result, we cannot rule out possible contributions by
688 magnetopause shadowing to the electron flux dropout event studied in this paper, particularly on
689 12-13 November, when the greatest solar wind dynamic pressure variations were observed.

690 Examining the THEMIS, Cluster, and GOES locations on 12-13 November, we see that
691 EMIC waves were observed mainly in the afternoon and dusk sectors at geosynchronous orbit
692 and beyond, over a region of several hours in local time and 2-4 R_E wide. The Van Allen Probes
693 appeared to have been located too far inside the magnetosphere to see this EMIC wave activity.
694 The local time of the Van Allen Probes apogee near dawn during this event may have been a
695 factor in the wave observations, as EMIC waves are typically thought of as being strongest at
696 dusk. The observed region of EMIC wave occurrence during this event is consistent with
697 statistical studies [*Anderson et al.*, 1992a; 1992b; *Usanova et al.*, 2012; *Min et al.*, 2012;
698 *Meredith et al.*, 2014]. Electron fluxes at geosynchronous orbit were already beginning to
699 decrease on 12 November 2012, in association with the EMIC waves, before the shock arrival at
700 2316 UT. This suggests the magnetosphere was already primed for development of a deep
701 electron dropout by pre-existing EMIC waves at the time of the shock arrival. In Figures 2 and
702 3, the occurrence of the EMIC waves at geosynchronous orbit appears well-correlated with the
703 development of the initial electron flux dropout at 0.8 MeV on 12-13 November, but as the
704 previous discussion shows it is likely that the variations in the 0.8 MeV electrons at GOES and
705 the 235 keV and 459 keV electrons at the Van Allen Probes were mainly caused by reversible
706 changes in the magnetic field configuration. The prolonged dropout in the 2.0 MeV electrons
707 indicates that a permanent loss of electrons developed over time scales of a few hours, which is
708 consistent with the time scales for scattering by EMIC waves [*Summers et al.*, 2007].

709 The observations during this event are somewhat different from other recent studies of
710 electron flux dropouts, which concluded that magnetopause shadowing is an important loss
711 mechanism for values of L or L* > 5 and that other processes, such as wave-particle interactions
712 with EMIC waves, may be more important for L<5 [e.g., *Bortnik et al.*, 2006; *Yu et al.*, 2013].
713 In the event studied here, there was little variation in the electron fluxes for L<5 and the losses of
714 relativistic electrons for L>5 may have resulted from a combination of wave-particle
715 interactions, changes to the magnetic field configuration, and magnetopause shadowing.
716
717 **6. Conclusions**
718 We conclude that the initial phase of the electron dropout observed by GOES 13, 14, and
719 15, and the Van Allen Probes on 12-13 November 2012 was caused by a combination of
720 adiabatic processes due to local stretching of the magnetic field near dusk, along with non-
721 adiabatic processes due to wave-particle interactions with the He^+ EMIC waves observed by
722 THEMIS, Cluster, and the three GOES satellites. Although no magnetopause crossings were
723 observed at geosynchronous orbit, we cannot rule out that magnetopause shadowing may have
724 played a role in the observed electron behavior during this event, due to the enhanced solar wind
725 dynamic pressure and the arrival of the CME on 12 November. After noon on 13 November, the
726 greater than 2 MeV electron fluxes remained at instrumental background levels, while the lower
727 energy electron fluxes recovered slightly. This brief recovery in the 0.8 MeV electrons at
728 geosynchronous orbit may have been caused by electron acceleration processes associated with
729 ULF waves and chorus observed by the Van Allen Probes, as well as changes in the magnetic
730 field configuration of the inner magnetosphere. The second phase of the dropout in the 0.8 MeV
731 electrons on 13-14 November 2012 appears to be mainly due to adiabatic processes such as

732 magnetic field stretching and the Dst effect in response to upstream solar wind drivers. As the
733 Dst index began to increase at the start of the storm recovery phase on 14 November, the particle
734 fluxes gradually increased to pre-storm values.
735
736 **Acknowledgments.** This work was performed under JHU/APL contract no. 921647 under
737 NASA Prime contract No. NAS5-01072. We acknowledge William Kurth for providing density
738 calculations from the EMFISIS data. RBSP-ECT funding was provided by JHU/APL Contract
739 No. 967399 under NASA's Prime Contract No. NAS5-01072. O. Santolík acknowledges
740 funding from the Czech Academy of Sciences through the Praemium Academiae award and from
741 the LH14010 grant. We acknowledge NASA contract NAS5-02099 and V. Angelopoulos for use
742 of data from the THEMIS Mission. Specifically: K. H. Glassmeier, U. Auster and W.
743 Baumjohann for the use of THEMIS FGM data provided under the lead of the Technical
744 University of Braunschweig and with financial support through the German Ministry for
745 Economy and Technology and the German Center for Aviation and Space (DLR) under contract
746 50 OC 0302. Data from the Van Allen Probes can be obtained through the Van Allen Probes
747 Science Gateway (http://rbspgway.jhuapl.edu/). GOES data are available from the NOAA
748 National Geophysical Data Center and the Preliminary Reports and Forecasts of Solar
749 Geophysical Data are available from the NOAA Space Weather Prediction Center. THEMIS
750 data are publicly available through the University of California Berkeley
751 (http://themis.ssl.berkeley.edu). Cluster data are available from the Cluster Science Archive.
752 Solar wind data and geomagnetic indexes are available online from NASA OMNIWeb. Wind
753 and ACE data are available online through CDAWeb.
754

References

Allen, R. C., J.-C. Zhang, L. M. Kistler, H. E. Spence, R.-L. Lin, B. Klecker, M. W. Dunlop, M. André, and V. K. Jordanova (2015), A statistical study of EMIC waves observed by Cluster 1: Wave properties, *J. Geophys. Res.*, *120*, doi:10.1002/2015JA021333.

Anderson, B., R. Erlandson, and L. Zanetti (1992a), A Statistical Study of Pc 1-2 Magnetic Pulsations in the Equatorial Magnetosphere, 2. Wave Properties, *J. Geophys. Res.*, *97*, 3089-3101.

Anderson, B., R. Erlandson, and L. Zanetti (1992b), A Statistical Study of Pc 1-2 Magnetic Pulsations in the Equatorial Magnetosphere, 1. Equatorial Occurrence Distributions, *J. Geophys. Res.*, *97*, 3075-3088.

Anderson, B. J. (1994), An overview of spacecraft observations of 10 s to 600 s period magnetic pulsations in the Earth's magnetosphere, in *Solar Wind Sources of Magnetospheric Ultra-Low-Frequency Waves*, *Geophys. Monogr. Ser., vol. 81*, edited by M. J. Engebretson, K. Takahashi, and M. Scholer, pp. 25-43, AGU, Washington, D.C.

Angelopoulos, V. (2008), The THEMIS Mission, *Space Sci. Rev.*, *141*, 5–34, doi: 10.1007/s11214-008-9336-1.

Auster, H. U., K. H. Glassmeier, W. Magnes, O. Aydogar, W. Baumjohann, D. Constantinescu, D. Fischer, K. H. Fornacon, E. Georgescu, P. Harvey, O. Hillenmaier, R. Kroth, M. Ludlam, Y.

778 Narita, R. Nakamura, K. Okrafka, F. Plaschke, I. Richter, H. Schwarzl, B. Stoll, A.
779 Valavanoglou, M. Wiedemann (2008), The THEMIS fluxgate magnetometer. *Space Sci. Rev.*,
780 *141*, 235-264, doi:10.1007/s11214-008-9365-9.
781
782 Baker, D. N., S. G. Kanekal, V. C. Hoxie, S. Batiste, M. Bolton, X. Li, S. R. Elkington, S. Monk,
783 R. Reukauf, S. Steg, J. Westfall, C. Belting, B. Bolton, D. Braun, B. Cervelli, K. Hubbell M.
784 Kien, S. Knappmiller, S. Wade, B. Lamprecht, K. Stevens, J. Wallace, A. Yehle, H.E. Spence, R.
785 Friedel (2012), The Relativistic Electron-Proton Telescope (REPT) Instrument on Board the
786 Radiation Belt Storm Probes (RBSP) Spacecraft: Characterization of Earth's Radiation Belt
787 High-Energy Particle Populations, *Space Sci. Rev*., doi:10.1007/s11214-012-9950-9.
788
789 Balogh, A., C. M., Carr, M. H. Acuña, M. W. Dunlop, T. J. Beek, P. Brown, K.-H. Fornaçon, E.
790 Georgescu, K.-H. Glassmeier, J. Harris, G. Musmann, T. Oddy, and K. Schwingenschuh (2001),
791 The Cluster Magnetic Field Investigation: overview of in-flight performance and initial results,
792 *Ann. Geophys.*, *19*, 1207-1217, doi:10.5194/angeo-19-1207-2001.
793
794 Barfield, J. N., and R. L. McPherron (1978), Stormtime Pc 5 magnetic pulsations observed at
795 synchronous orbit and their correlation with the partial ring current, *J. Geophys. Res., 83*, 739-
796 743.
797
798 Blake, J. B., P. A. Carranza, S. G. Claudepierre, J. H. Clemmons, W. R. Crain Jr., Y. Dotan, J.F.
799 Fennell, F.H. Fuentes, R.M. Galvan, J.S. George, M.G. Henderson, M. Lalic, A.Y. Lin, M.D.
800 Looper, D.J. Mabry, J.E. Mazur, B. McCarthy, C.Q. Nguyen, T.P. O'Brien, M.A. Perez, M.T.

801 Redding, J.L. Roeder, D.J. Salvaggio, G.A. Sorensen, H.E. Spence, S. Yi, M. P. Zakrzewski
802 (2013), The Magnetic Electron Ion Spectrometer (MagEIS) Instruments Aboard the Radiation
803 Belt Storm Probes (RBSP) Spacecraft, *Space Sci. Rev.*, doi:10.1007/s11214-013-9991-8.
804
805 Bortnik, J., R. M. Thorne, T. P. O'Brien, J. C. Green, R. J. Strangeway, Y. Y. Shprits, and D. N.
806 Baker (2006), Observation of two distinct, rapid loss mechanisms during the 20 November 2003
807 radiation belt dropout event, *J. Geophys. Res.*, *111*, A12216, doi:10.1029/2006JA011802.
808
809 Bräysy, T., K. Mursula, and G. Marklund (1998), Ion cyclotron waves during a great magnetic
810 storm observed by Freja double-probe electric field instrument, *J. Geophys. Res.*, *103*, 4145-
811 4155.
812
813 Brueckner, G. E., R. A. Howard, M. J. Koomen, C. M. Korendyke, D. J. Michels, J. D. Moses,
814 D. G. Socker, K. P. Dere, P. L. Lamy, A. Llebaria, M. V. Bout, R. Schwenn, G. M. Simnett, D.
815 K. Bedford, C. J. Eyles (1995), The Large Angle Spectroscopic Coronagraph (LASCO), *Solar*
816 *Physics*, 162, 357-402.
817
818 Engebretson, M. J., D. L. Murr, K. N. Erickson, R. J. Strangeway, D. M. Klumpar, S. A.
819 Fuselier, L. J. Zanetti, and T. A. Potemra (1992), The spatial extent of radial magnetic pulsation
820 events observed in the dayside near synchronous orbit, *J. Geophys. Res.*, *97*, 13741-13758.
821
822 Eriksson, P. T. I., L. G. Blomberg, A. D. M. Walker, and K. -H. Glassmeier (2005), Poloidal
823 ULF oscillations in the dayside magnetosphere: a Cluster study, *Ann. Geophys.*, *23*, 2679-2686.

824

825 Eriksson, P. T. I., L. G. Blomberg, S. Schaefer, and K. -H. Glassmeier (2008), Sunward
826 propagating Pc5 waves observed on the post-midnight magnetospheric flank, *Ann. Geophys.*, *2*6,
827 1567-1579.

828

829 Fraser, B. J., R. S. Grew, S. K. Morley, J. C. Green, H. J. Singer, T. M. Loto'aniu, and M. F.
830 Thomsen (2010), Storm time observations of electromagnetic ion cyclotron waves at
831 geosynchronous orbit: GOES results, *J. Geophys. Res.*, *115*, A05208,
832 doi:10.1029/2009JA014516.

833

834 Green, J. C., T. G. Onsager, T. P. O'Brien, and D. N. Baker (2004), Testing loss mechanisms
835 capable of rapidly depleting relativistic electron flux in the Earth's outer radiation belt, *J.*
836 *Geophys. Res.*, *109*, A12211, doi:10.1029/2004JA010579.

837

838 Gurnett, D. A., and A. Bhattacharjee (2005), *Introduction to Plasma Physics with Space and*
839 *Laboratory Applications, Cambridge University Press*, New York.

840

841 Halford, A., B. J. Fraser, and S. K. Morley (2015), EMIC waves and plasmaspheric plume
842 density: CRRES results, *J. Geophys. Res*., *120*, doi:10.1002/2014JA020338.

843 Hughes, J. W. (1994), Magnetospheric ULF waves: A tutorial with a historical perspective, in
844 *Solar Wind Sources of Magnetospheric Ultra-Low-Frequency Waves*, *Geophys. Monogr. Ser.*,
845 *vol. 81*, edited by M. J. Engebretson, K. Takahashi, and M. Scholer, pp. 1-11, AGU, Washington,
846 D.C.

Howard, R. A., J. D. Moses, A. Vourlidas, J. S. Newmark, D. G. Socker, S. P. Plunkett, C. M. Korendyke, J. W. Cook, A. Hurley, J. M. Davila, W. T. Thompson, O. C. St Cyr, E. Mentzell, K. Mehalick, J. R. Lemen, J. P. Wuelser, D. W. Duncan, T. D. Tarbell, C. J. Wolfson, A. Moore, R. A. Harrison, N. R. Waltham, J. Lang, C. J. Davis, C. J. Eyles, H. Mapson-Menard, G. M. Simnett, J. P. Halain, J. M. Defise, E. Mazy, P. Rochus, R. Mercier, M. F. Ravet, F. Delmotte, F. Auchere, J. P. Delaboudiniere, V. Bothmer, W. Deutsch, D. Wang, N. Rich, S. Cooper, V. Stephens, G. Maahs, R. Baugh, D. McMullin, T. Carter (2008), Sun Earth Connection Coronal and Heliospheric Investigation (SECCHI), *Space Science Reviews*, *136,* 67-115, doi:10.1007/s11214-008-9341-4.

Jacobs, J. A., Y. Kato, S. Matsushita, and V. A. Troitskaya (1964), Classification of geomagnetic micropulsations, *J. Geophys. Res.*, *69*, 180-181.

King, J. H. and N. E. Papitashvili (2005), Solar wind spatial scales in and comparisons of hourly Wind and ACE plasma and magnetic field data, *J. Geophys. Res.*, *110*, A02104, doi:10.1029/2004JA010649.

Kozyra, J., T. Cravens, A. Nagy, E. Fontheim, and R. Ong (1984), Effects of Energetic Heavy Ions on Electromagnetic Ion Cyclotron Wave Generation in the Plasmapause Region, *J. Geophys. Res.*, *89*, 2217-2233.

869 Kim, H.-J., and A. A. Chan (1997), Fully adiabatic changes in storm time relativistic electron
870 fluxes*, J. Geophys. Res., 102*(A10), 22107–22116, doi:10.1029/97JA01814.
871
872 Kim, K. C., D.-Y. Lee, H.-J. Kim, L. R. Lyons, E. S. Lee, M. K. Öztürk, and C. R. Choi (2008),
873 Numerical calculations of relativistic electron drift loss effect, *J. Geophys. Res*., *113*, A09212,
874 doi:10.1029/2007JA013011.
875
876 Kim, K. C., D.-Y. Lee, H.-J. Kim, E. S. Lee, and C. R. Choi (2010), Numerical estimates of drift
877 loss and Dst effect for outer radiation belt relativistic electrons with arbitrary pitch angle, *J.*
878 *Geophys. Res.*, *115*, A03028, doi:10.1029/2009JA014523.
879
880 Kletzing, C. A., W.S. Kurth, M. Acuna, R. J. MacDowall, R. B. Torbert, T. Averkamp, D. Bodet,
881 S. R. Bounds, M. Chutter, J. Connerney, D. Crawford, J. S. Dolan, R. Dvorsky, G. B.
882 Hospodarsky, J. Howard, V. Jordanova, R. A. Johnson, D. L. Kirchner, B. Mokrzycki, G.
883 Needell, J. Odom, D. Mark, R. Pfaff, J. R. Phillips, C. W. Piker, S. L. Remington, D. Rowland,
884 O. Santolik, R. Schnurr, D. Sheppard, C. W. Smith, R. M. Thorne, J. Tyler (2013), The Electric
885 and Magnetic Field Instrument Suite and Integrated Science (EMFISIS) on RBSP, *Space Sci.*
886 *Rev.*, *179*, 127-181, doi: 10.1007/s11214-013-9993-6.
887
888 Kurth, W. S., S. De Pascuale, J. B. Faden, C. A. Kletzing, G. B. Hospodarsky, S. Thaller, and J.
889 R. Wygant (2015), Electron densities inferred from plasma wave spectra obtained by the Waves
890 instrument on Van Allen Probes, *J. Geophys. Res.*, *120*, 904–914, doi:10.1002/2014JA020857.
891

892 Li, X., D. N. Baker, M. Temerin, T. E. Cayton, E. G. D. Reeves, R. A. Christensen, J. B. Blake,
893 M. D. Looper, R. Nakamura, and S. G. Kanekal (1997), Multisatellite observations of the outer
894 zone electron variation during the November 3–4, 1993, magnetic storm, *J. Geophys. Res.,*
895 *102*(A7), 14123–14140, doi:10.1029/97JA01101.
896
897 Liu, W., T. E. Sarris, X. Li, S. R. Elkington, R. Ergun, V. Angelopoulos, J. Bonnell, and K. H.
898 Glassemeier (2009), Electric and magnetic field observations of Pc4 and Pc5 pulsations in the
899 inner magnetosphere: A statistical study, *J. Geophys. Res.*, *114,* A12206,
900 doi:10.1029/2009JA014243.
901
902 Lopez, R. E., Lui, A. T. Y., Sibeck, D. G., McEntire, R. W., Zanetti, L. J., Potemra, T. A., and
903 Krimigis, S. M. (1988), The longitudinal and radial distribution of magnetic reconfigurations in
904 the near-Earth magnetotail as observed by AMTE/CCE, *J. Geophys. Res*., *93*, 997–1001.
905
906 Matsumura, C., Y. Miyoshi, K. Seki, S. Saito, V. Angelopoulos, and J. Koller (2011), Outer
907 radiation belt boundary location relative to the magnetopause: Implications for magnetopause
908 shadowing, *J. Geophys. Res.*, *116*, A06212, doi:10.1029/2011JA016575.
909
910 Meredith N. P., R. B. Horne, T. Kersten, B. J. Fraser, and R. S. Grew (2014), Global morphology
911 and spectral properties of EMIC waves derived from CRRES observations, *J. Geophys. Res.*,
912 *119*, 5328-5342, doi:10.1002/2014JA020064.
913

914 Meredith, N. P., R. M. Thorne, R. B. Horne, D. Summers, B. J. Fraser, and R. R. Anderson
915 (2003), Statistical analysis of relativistic electron energies for cyclotron resonance with EMIC
916 waves observed on CRRES, *J. Geophys. Res.*, *108*(A6), 1250, doi:10.1029/2002JA009700.
917
918 Millan, R. M., and R. M. Thorne (2007), Review of radiation belt relativistic electron losses, *J.*
919 *Atmos. Sol. Terr. Phys.*, *69*, 362-377, doi:10.1016/j.jastp.2006.06.019.
920
921 Min, K., J. Lee, K. Keika, and W. Li (2012), Global distribution of EMIC waves derived from
922 THEMIS observations, *J. Geophys. Res.*, *117*, A05219, doi:10.1029/2012JA017515.
923
924 Morley, S. K., S. T. Ables, M. D. Sciffer, and B. J. Fraser (2009), Multipoint observations of
925 Pc1-2 waves in the afternoon sector, *J. Geophys. Res.*, *114*, A09205,
926 doi:10.1029/2009JA014162.
927
928 Morley, S. K., R. H. W. Friedel, E. L. Spanswick, G. D. Reeves, J. T. Steinberg,
929 J. Koller, T. E. Cayton, and E. Noveroske (2010), Dropouts of the outer electron radiation belt in
930 response to solar wind stream interfaces: Global Positioning System Observations, Proc. R. Soc.
931 A., 466, 3329-3350, doi:10.1098/rspa.2010.0078.
932
933 Onsager, T. G., G. Rostoker, H.-J. Kim, G. D. Reeves, T. Obara, H. J. Singer, and C. Smithro
934 (2002), Radiation belt electron flux dropouts: Local time, radial, and particle-energy dependence,
935 *J. Geophys. Res.*, *107*(A11), 1382, doi:10.1029/2001JA000187.
936

937 Parks, George K., *Physics of Space Plasmas* (1991), Addison-Wesley Publishing Company, New
938 York.
939
940 Paulson, K.W., C. W. Smith, M. R. Lessard, M. J. Engebretsen, R. B. Torbert, and C. A.
941 Kletzing (2014), In situ observations of Pc1 pearl pulsations by the Van Allen Probes, *Geophys.*
942 *Res. Lett.*, *41*, 1823-1829, doi:10.1002/2013GL059187.
943
944 Reeves, G. D., K. L. McAdams, R. H. W. Friedel, and T. P. O'Brien (2003), Acceleration and
945 loss of relativistic electrons during geomagnetic storms, *Geophys. Res. Lett.*, *30*(10), 1529, doi:
946 10.1029/2002GL0165013.
947
948 Reeves, G. D. (1998), Relativistic electrons and magnetic storms: 1992-1995, *Geophys. Res.*
949 *Lett.*, *25*, 1817-1820.
950
951 Santolík, O., E. Lefeuvre, M. Parrot, and J. L. Rauch (2001), Complete wave-vector directions of
952 electromagnetic emissions: Application to INTERBALL-2 measurements in the nightside auroral
953 zone, *J. Geophys. Res.*, *106*(A7), 13191-13201.
954
955 Santolík, O., J. S. Pickett, D. A. Gurnett, and L. R. O. Storey (2002), Magnetic component of
956 narrowband ion cyclotron waves in the auroral zone, *J. Geophys. Res.*, *107*(A12), 1444,
957 doi:10.1029/2001JA000146.
958

959 Santolík, O., M. Parrot, F. Lefeuvre (2003) Singular value decomposition methods for wave
960 propagation analysis, *Radio Science*, 38(1), 1010.
961
962 Sigsbee, K., Slavin, J. A., Lepping, R. P., Szabo, A., Øieroset, M., Kaiser, M. L., Reiner, M. J.,
963 and Singer, H. J. (2005), Statistical and superposed epoch study of dipolarization events using
964 data from Wind perigee passes, *Ann. Geophys.*, *23*, 831-851, doi:10.5194/angeo-23-831-2005.
965
966 Summers, D., B. Ni, and N. P. Meredith (2007), Timescales for radiation belt electron
967 acceleration and loss due to resonant wave-particle interactions: 2. Evaluation for VLF chorus,
968 ELF hiss, and electromagnetic ion cyclotron waves, *J. Geophys. Res.*, *112*, A04207,
969 doi:10.1029/2006JA011993.
970
971 Takahashi, K., R. W. McEntire, A. T. Y. Lui, and T. A. Potemra (1990), Ion flux oscillations
972 associated with a radially polarized transverse Pc 5 magnetic pulsation, *J. Geophys. Res.*, *95*,
973 3717-3731.
974
975 Takahashi, K., R. E. Denton, W. Kurth, C. Kletzing, J. Wygant, J. Bonnell, L. Dai, K. Min, C.
976 W. Smith, and R. MacDowell (2015), Externally driven plasmaspheric ULF waves observed by
977 the Van Allen Probes, *J. Geophys. Res*., *120*, 526-522, doi:10.1002/2014JA020373.
978
979 Thorne, R., and C. Kennel (1971), Relativistic Electron Precipitation during Magnetic Storm
980 Main Phase, *J. Geophys. Res.*, *76*, 4446-4453.
981

982 Thorne, R., and R. Horne (1994), Energy Transfer Between Energetic Ring Current H+ and O+
983 by Electromagnetic Ion Cyclotron Waves, *J. Geophys. Res.*, *99*, 17275-17282.
984
985 Turner, D. L., S. K. Morley, Y. Miyoshi, B. Ni, and C.-L. Huang (2013), Outer Radiation Belt
986 Flux Dropouts: Current Understanding and Unresolved Questions, in *Dynamics of the Earth's*
987 *Radiation Belts and Inner Magnetosphere*, pp. 195-212, *Geophysical Monograph Series 199*, D.
988 Summers, I. R. Mann, D. N. Baker, and M. Schulz, editors, American Geophysical Union,
989 Washington D.C., doi:10.1029/2012GM001310.
990
991 Turner, D. L., Y. Shprits, M. Hartinger, and V. Angelopoulos (2012), Explaining sudden losses
992 of outer radiation belt electrons during geomagnetic storms, *Nature Physics*, *8*,
993 doi:10.1038/NPHS2185.
994
995 Usanova, M. E., I. R. Mann, J. Bortnik, L. Shao, and V. Angelopoulos (2012), THEMIS
996 observations of electromagnetic ion cyclotron wave occurrence: Dependence on AE, SYMH, and
997 solar wind dynamic pressure*, J. Geophys. Res.*, *117*, A10218, doi:10.1029/2012JA018049.
998
999 Walsh, B. M., D. G. Sibeck, Y. Nishimura, and V. Angelopoulos (2013), Statistical analysis of
1000 the plasmaspheric plume at the magnetopause, *J. Geophys. Res.*, *118*, 4844-4851,
1001 doi:10.1002/jgra.50458.
1002
1003 West, H. I., R. M. Buck, and J. R. Walton (1972), Shadowing of Electron Azimuthal-Drift
1004 Motions near the Noon Magnetopause, *Nature Physical Science*, 240, 6-7.

1005

1006 Yu, Y., J. Koller, and S. K. Morley (2013), Quantifying the effect of magnetopause shadowing
1007 on electron radiation belt dropouts, *Ann. Geophys.*, *31*, 1929-1939, doi:10.5194/angeo-31-1929-
1008 2013.

1009

1010 Yuan, Z., X. Deng, X. Lin, Y. Peng, M. Zhou, P. M. E. Décréau, J. G. Trotignon, E. Lucek, H.
1011 U. Frey, and J. Wang (2012), Link between EMIC waves in plasmaspheric plume and a detached
1012 sub-auroral proton arc with observations of Cluster and IMAGE satellites, *Geophys. Res. Lett.*,
1013 *37*, L07108, doi:10.1029/2010GL042711.

1014

1015 Yuan, Z., M. Li, Y. Xiong, H. Li, M. Zhou, D. Wang, S. Huang, X. Deng, and J. Wang (2013),
1016 Simultaneous observations of precipitating radiation belt electrons and ring current ions
1017 associated with the plasmaspheric plume, *J. Geophys. Res.*, *118*, 4391-4399,
1018 doi:10.1029/jgra.50432.

1019

1020

1021

1022

1023

1024

1025

1026

1027 **Figure Captions**

Figure 1. An overview of the geomagnetic activity on 12-15 November 2012. The top four panels show OMNI solar wind flow speed, dynamic pressure, interplanetary magnetic field (IMF) Bz in GSM coordinates, and the solar wind clock and cone angles. All OMNI parameters have been propagated to the Earth's bow shock. The next two panels show the 0.8 MeV and 2.0 MeV electron fluxes measured by GOES 13, 14 and 15. The final three panels show the REPT electrons for energies of 2.0 MeV from Van Allen Probe B (RBSP-B) as a function of L shell and time, the Dst index, and the Kp index. The times of the shock arrival on 12 November at 2316 UT, and the time of the solar wind sector boundary on 14 November at 0336 UT have been marked with magenta lines.

Figure 2. The portions of the orbits of GOES 13, 14, and 15, and of THEMIS and Cluster 2 when EMIC waves were observed on 12-13 November as a function of L shell and MLT. The start of each trajectory is marked with a star and dots are placed for every hour and 30 minutes after the hour.

Figure 3. FFT spectrograms of the GOES 15 parallel, eastward, and radial wave magnetic fields. Magenta lines for the O^+, He^+, and H^+ ion gyrofrequencies have been overplotted on the spectrograms. The bottom two panels show the 0.8 and 2.0 MeV electron fluxes and the magnetic field inclination angle at GOES 15. The times of the shock arrival on 12 November at 2316 UT and the solar wind sector boundary crossing on 14 November at 0336 UT have been marked with a vertical magenta line.

Figure 4. FFT spectrograms of the GOES 14 wave magnetic fields in field-aligned coordinates and GOES 14 electron fluxes. The format is the same as Figure 3. The times at which GOES 14 was located at 16 LT and 19 LT have also been marked with vertical magenta lines.

Figure 5. FFT spectrograms of the GOES 13 wave magnetic fields in field-aligned coordinates and GOES 13 electron fluxes. The format is the same as Figures 3 and 4. The times at which GOES 13 was located at 16 LT and 19 LT have been marked with vertical magenta lines.

Figure 6. FFT spectrograms of the Van Allen Probe B (RBSP-B) wave magnetic fields in field-aligned coordinates showing ULF wave observations for 12-14 November. A magenta line for the O^+ ion gyrofrequency has been overplotted on the spectrograms.

Figure 7. The THEMIS-A FGL magnetic field in field-aligned coordinates shortly after the shock arrival on 13 November 2012. Magenta lines for the O^+, He^+, and H^+ ion gyrofrequencies have been overplotted on the spectrograms.

Figure 8. EMIC waves observed by the Cluster 2 FGM on 13 November around 0630 UT near 17 LT. The magnetic fields are in field-aligned coordinates.

Figure 9. Results of wave normal analysis for GOES 15 on 12-13 November using PRASSADCO. From top to bottom are the total magnetic field power, the ellipticity, the wave normal angle, planarity, and solar wind dynamic pressure. Values of the ellipticity equal to -1 indicate left hand polarization, +1 indicates right hand polarization, and 0 indicates linear

1074 polarization. When the wave normal angle theta is 0°, the waves propagate parallel or anti-
1075 parallel to the magnetic field, and when it is 90°, the waves propagate perpendicular to the
1076 magnetic field. The ellipticity, wave normal angle, and planarity are shown only for total
1077 magnetic field power greater than 10^{-2} nT^2/Hz and planarity greater than 0.5. The ion cyclotron
1078 frequencies and CME arrival time have been marked on the plots.
1079
1080 **Figure 10.** Electron observations from Van Allen Probe B (RBSP-B) as a function of L shell
1081 and MLT for 12-14 November 2012. From top to bottom the energies are 134 keV, 235 keV,
1082 459 keV, 875 keV, 1040 keV and 2 MeV.

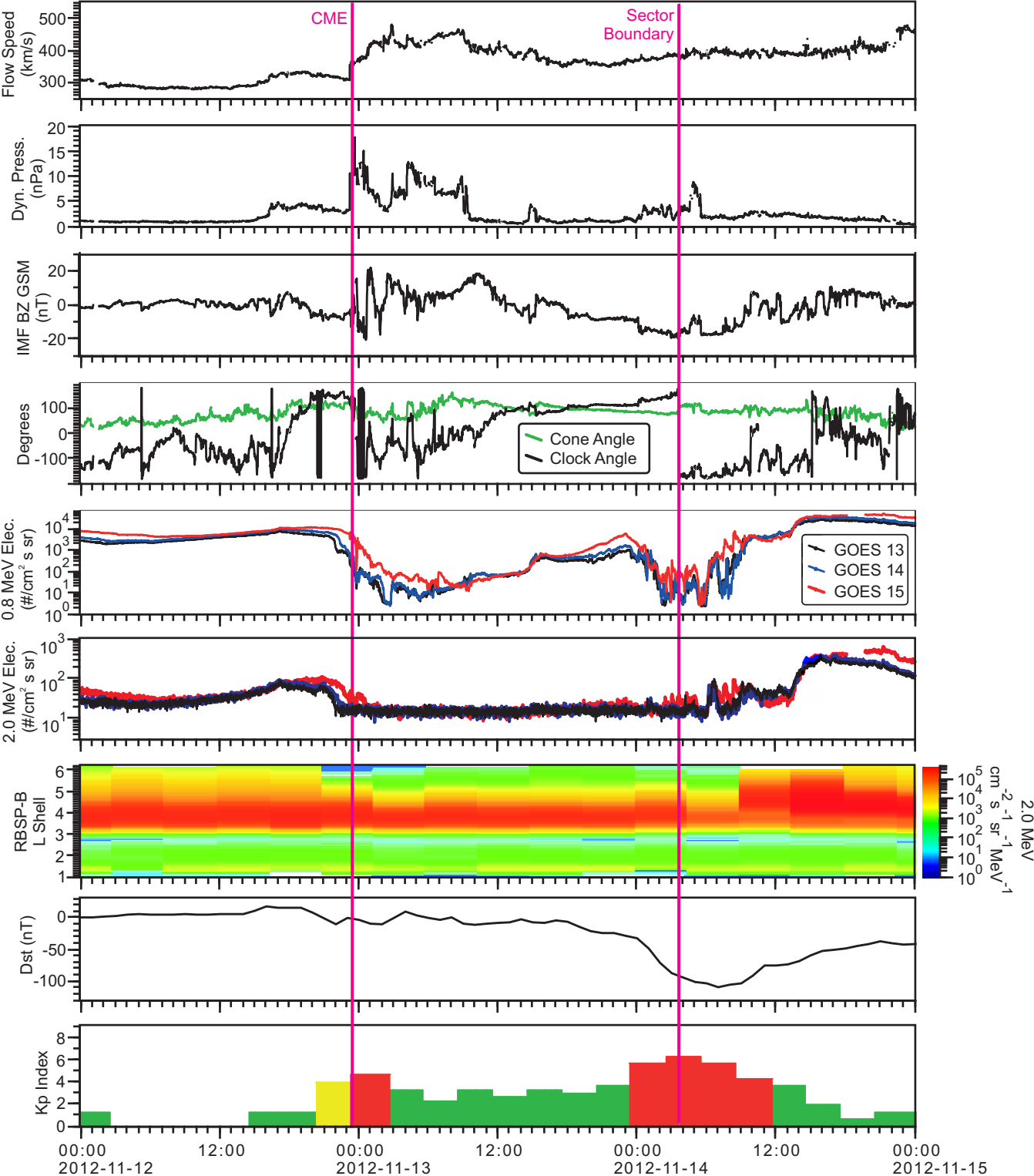
CME
Sector Boundary
Flow Speed (km/s)
500
400
300
Dyn. Press. (nPa)
20
15
10
5
0
IMF BZ GSM (nT)
20
0
-20
Degrees
100
0
-100
Cone Angle
Clock Angle
0.8 MeV Elec. (#/cm² s sr)
GOES 13
GOES 14
GOES 15
2.0 MeV Elec. (#/cm² s sr)
RBSP-B L Shell
2.0 MeV cm⁻² s⁻¹ sr⁻¹ MeV⁻¹
Dst (nT)
0
-50
-100
Kp Index
8
6
4
2
0
00:00 2012-11-12
12:00
00:00 2012-11-13
12:00
00:00 2012-11-14
12:00
00:00 2012-11-15

GOES, Cluster, and THEMIS
EMIC Wave Observations 2012-11-12 to 2012-11-13

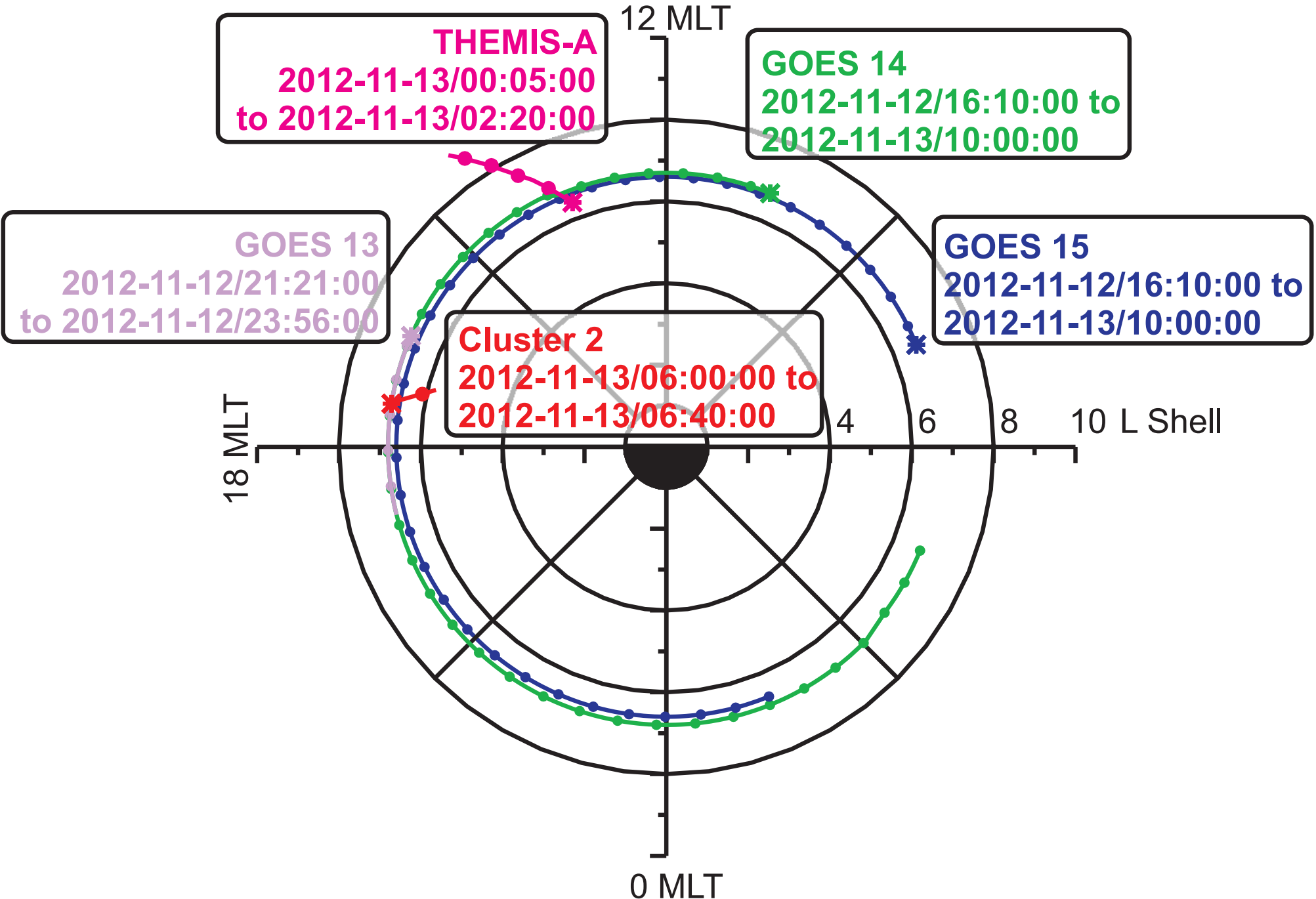

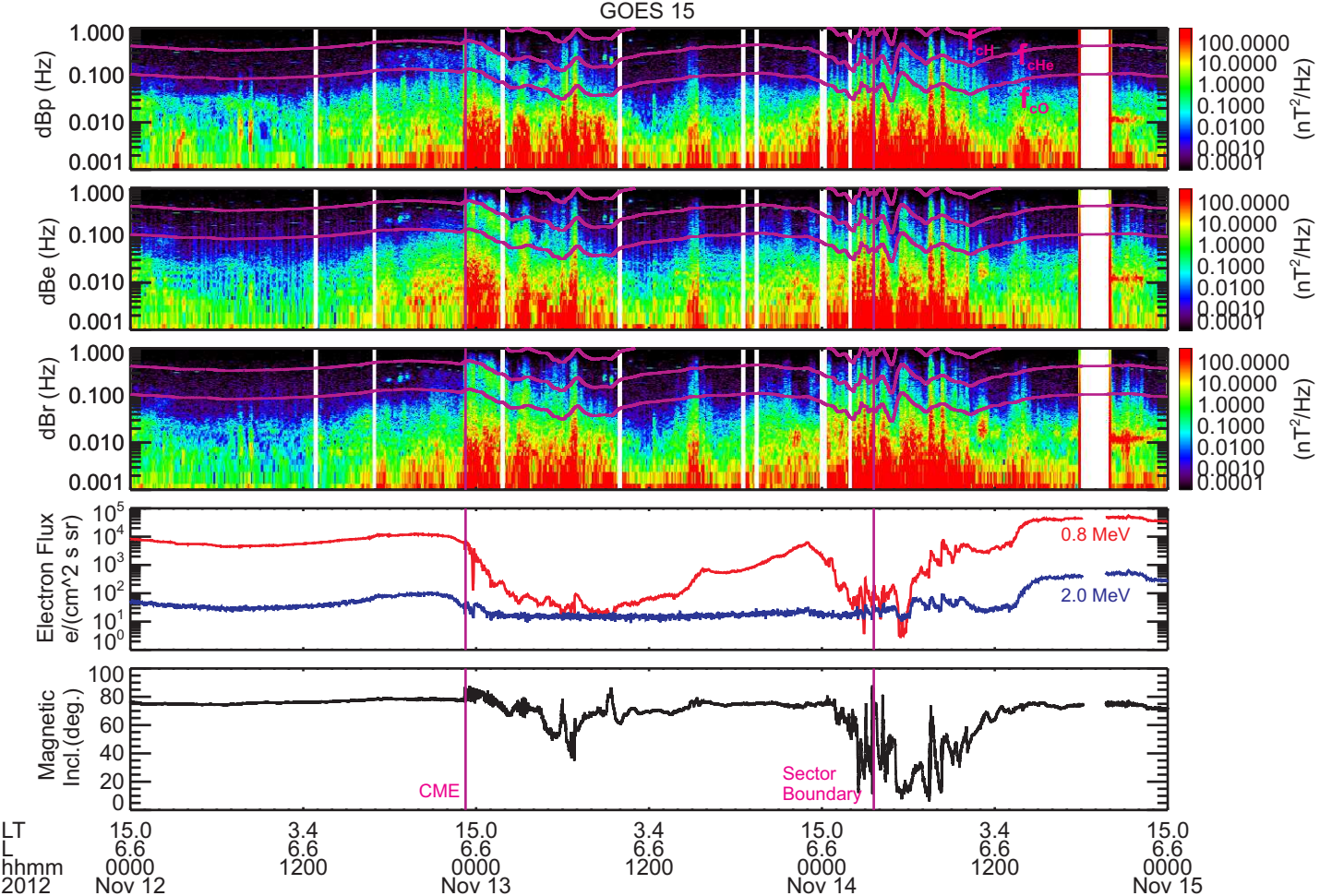
GOES 15
dBp (Hz)
dBe (Hz)
dBr (Hz)
1.000
0.100
0.010
0.001
fcH
fcHe
fcO
100.0000
10.0000
1.0000
0.1000
0.0100
0.0010
0.0001
(nT²/Hz)
Electron Flux
e/(cm^2 s sr)
0.8 MeV
2.0 MeV
Magnetic
Incl.(deg.)
CME
Sector
Boundary
LT
L
hhmm
2012
15.0
6.6
0000
Nov 12
3.4
6.6
1200
Nov 13
Nov 14
Nov 15

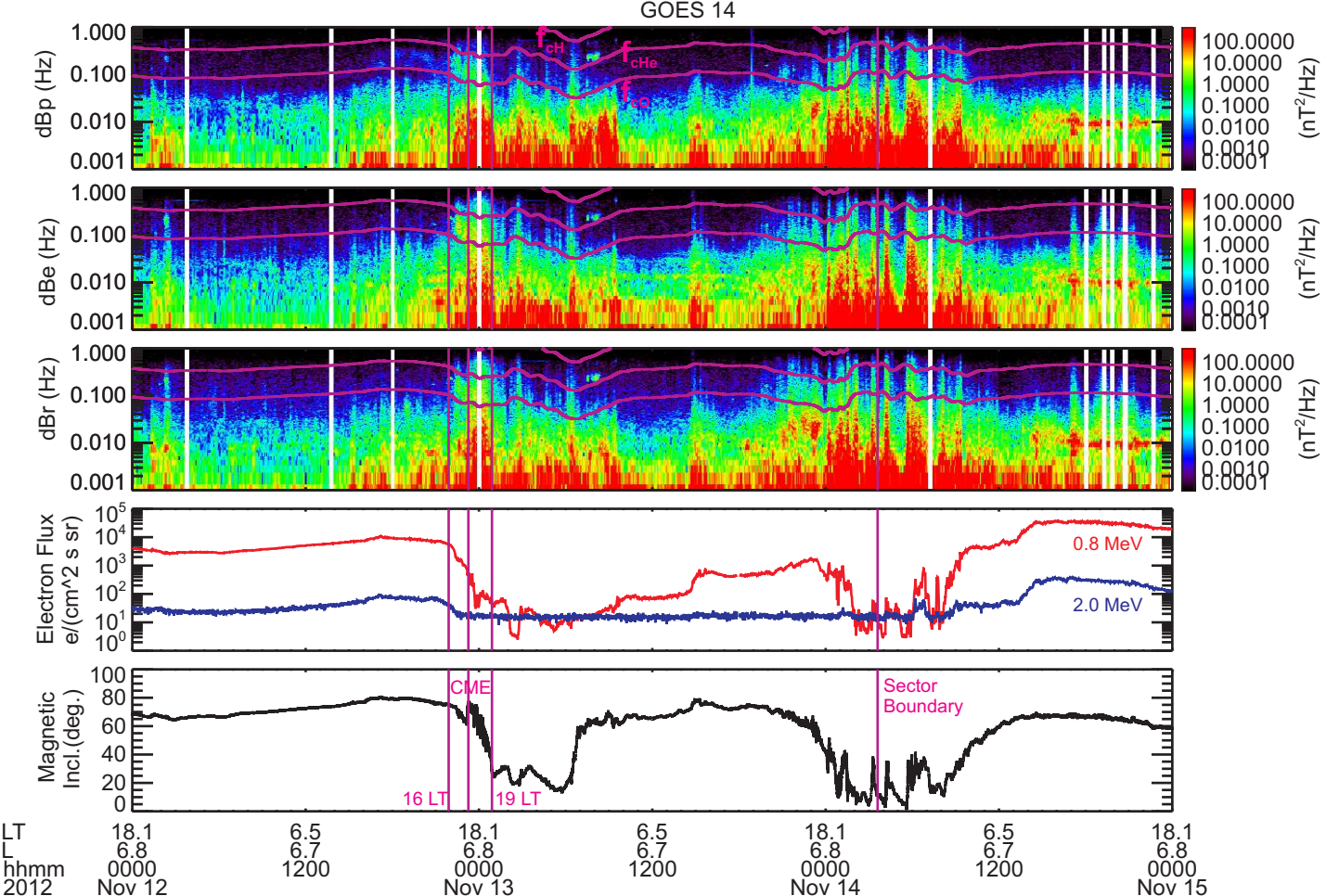
GOES 14
dBp (Hz)
dBe (Hz)
dBr (Hz)
1.000
0.100
0.010
0.001
f_{cH}
f_{cHe}
f_{cO}
100.0000
10.0000
1.0000
0.1000
0.0100
0.0010
0.0001
(nT²/Hz)
Electron Flux
e/(cm^2 s sr)
0.8 MeV
2.0 MeV
Magnetic
Incl.(deg.)
CME
Sector
Boundary
16 LT
19 LT
LT
L
hhmm
2012
18.1
6.8
0000
Nov 12
6.5
6.7
1200
Nov 13
Nov 14
Nov 15

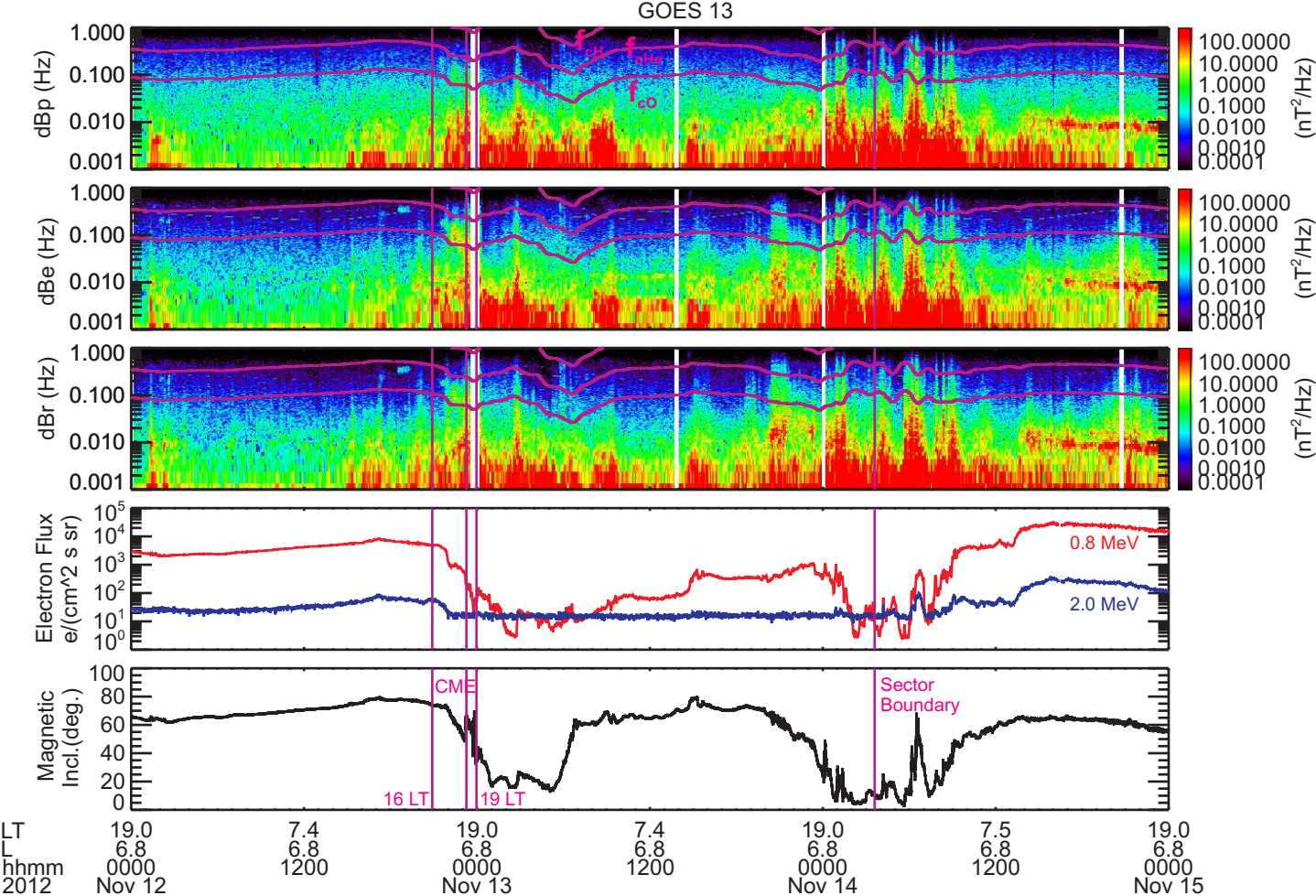
GOES 13
dBp (Hz)
dBe (Hz)
dBr (Hz)
1.000
0.100
0.010
0.001
f_{cH}
f_{cHe}
f_{cO}
100.0000
10.0000
1.0000
0.1000
0.0100
0.0010
0.0001
(nT²/Hz)
Electron Flux
e/(cm^2 s sr)
10^5
10^4
10^3
10^2
10^1
10^0
0.8 MeV
2.0 MeV
Magnetic
Incl.(deg.)
100
80
60
40
20
0
CME
Sector
Boundary
16 LT
19 LT
LT
L
hhmm
2012
19.0
6.8
0000
Nov 12
7.4
6.8
1200
19.0
6.8
0000
Nov 13
7.4
6.8
1200
19.0
6.8
0000
Nov 14
7.5
6.8
1200
19.0
6.8
0000
Nov 15

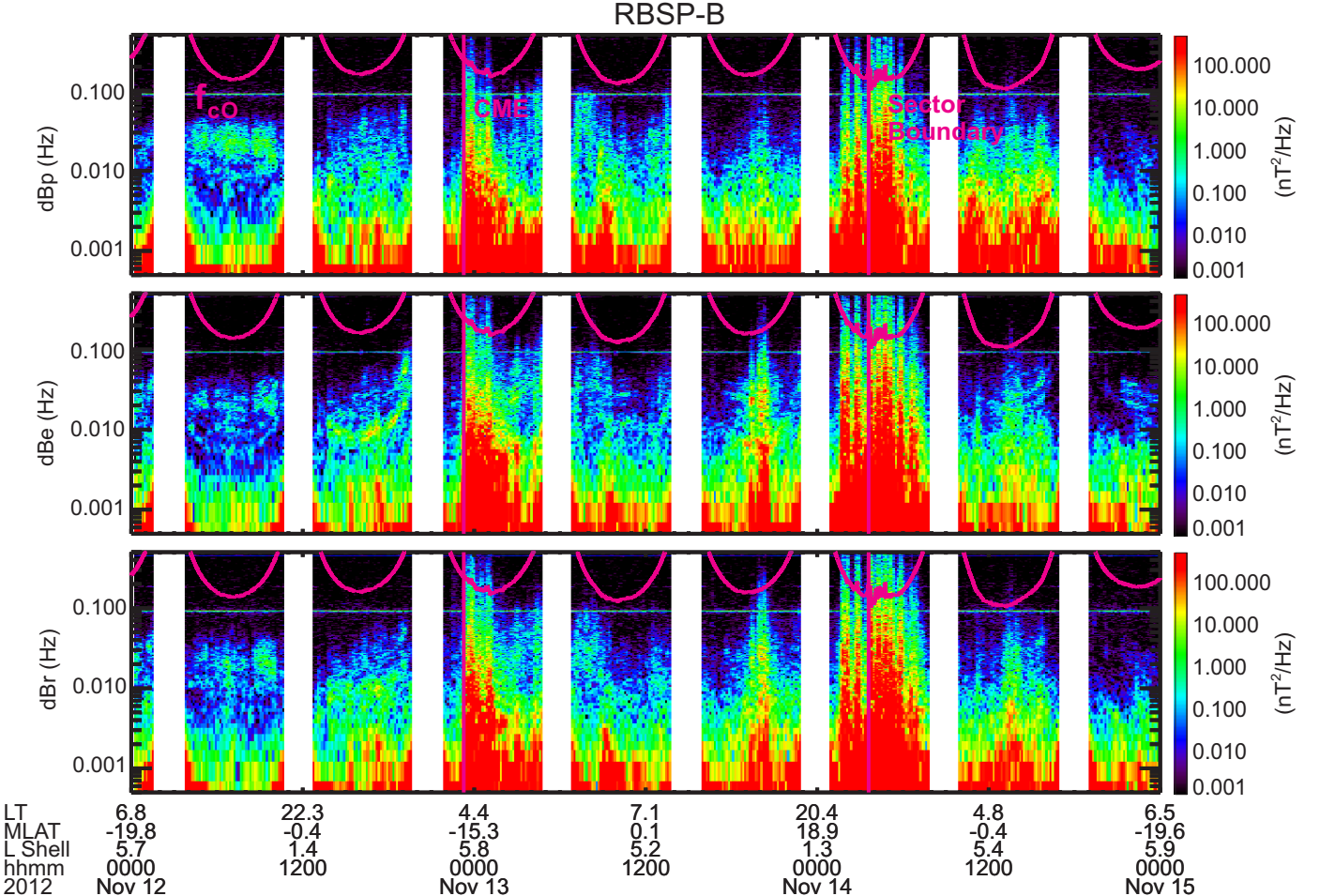
RBSP-B
dBp (Hz)
dBe (Hz)
dBr (Hz)
0.100
0.010
0.001
f_{cO}
CME
Sector Boundary
100.000
10.000
1.000
0.100
0.010
0.001
(nT²/Hz)
LT 6.8 22.3 4.4 7.1 20.4 4.8 6.5
MLAT -19.8 -0.4 -15.3 0.1 18.9 -0.4 -19.6
L Shell 5.7 1.4 5.8 5.2 1.3 5.4 5.9
hhmm 0000 1200 0000 1200 0000 1200 0000
2012 Nov 12 Nov 13 Nov 14 Nov 15

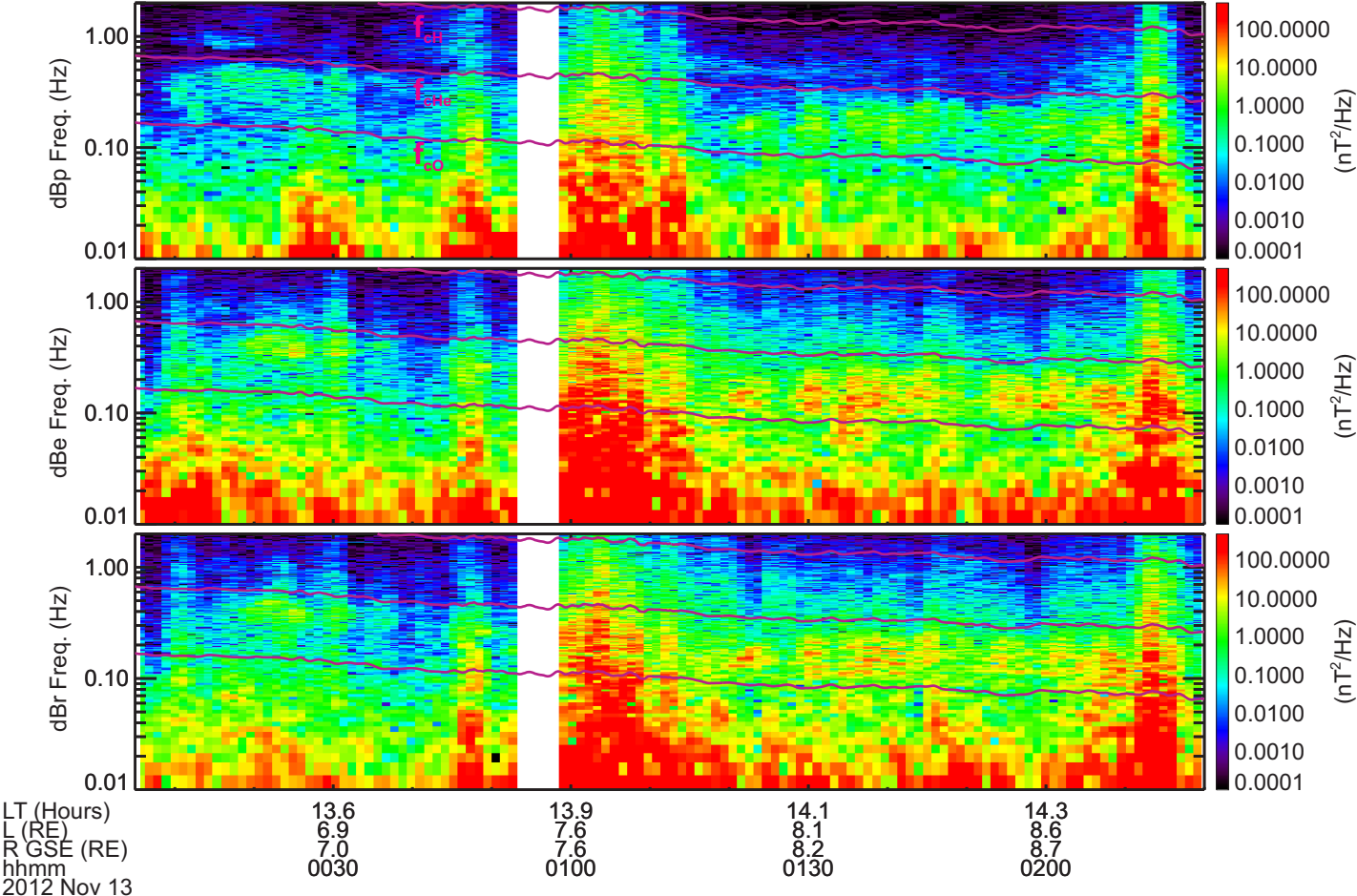
dBp Freq. (Hz)
dBe Freq. (Hz)
dBr Freq. (Hz)
1.00
0.10
0.01
f_{LH}
f_{cHe}
f_{co}
100.0000
10.0000
1.0000
0.1000
0.0100
0.0010
0.0001
(nT²/Hz)
LT (Hours) 13.6 13.9 14.1 14.3
L (RE) 6.9 7.6 8.1 8.6
R GSE (RE) 7.0 7.6 8.2 8.7
hhmm 0030 0100 0130 0200
2012 Nov 13

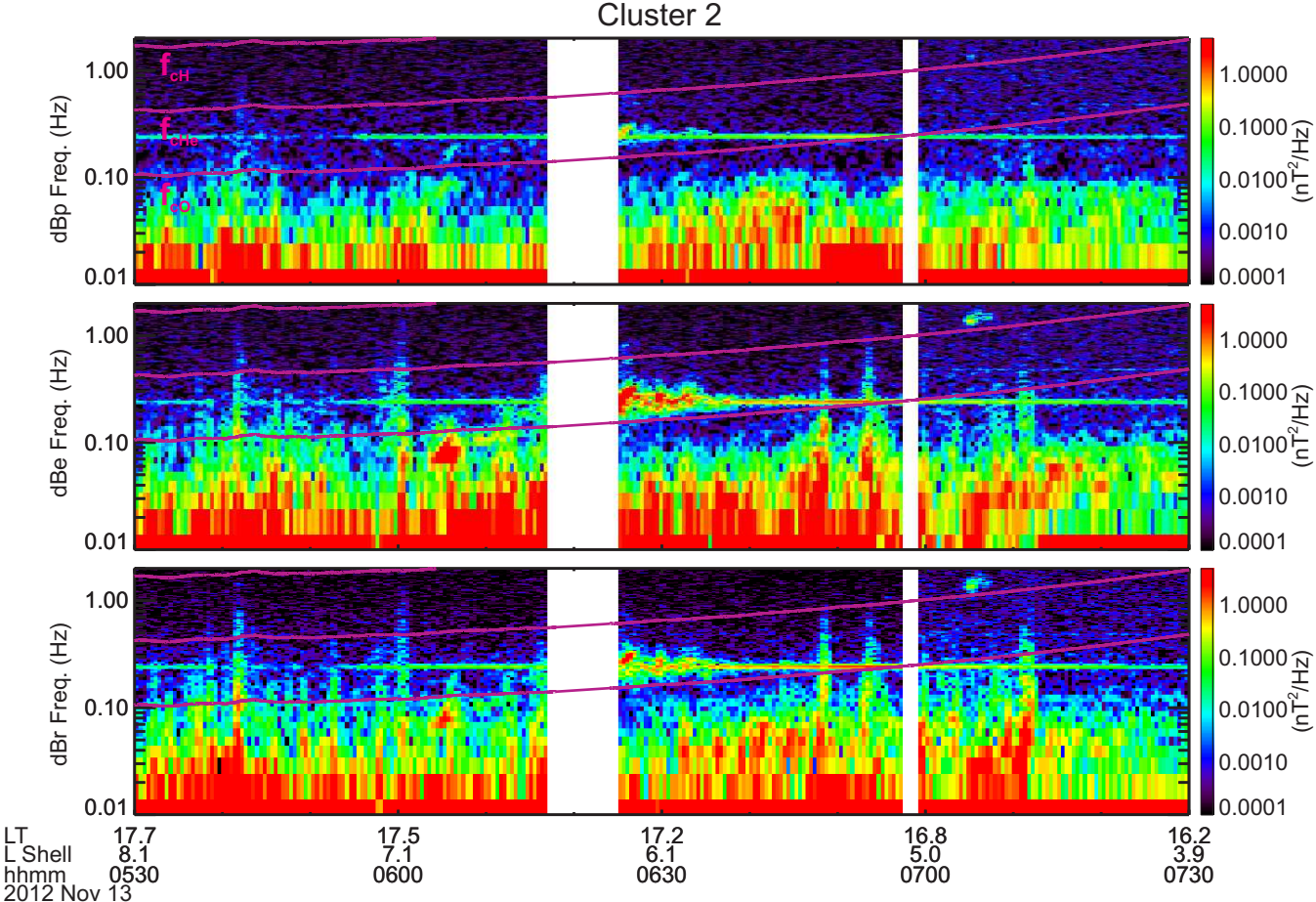
Cluster 2
dBp Freq. (Hz)
dBe Freq. (Hz)
dBr Freq. (Hz)
1.00
0.10
0.01
f_{cH}
f_{cHe}
f_{cO}
1.0000
0.1000
0.0100
0.0010
0.0001
(nT^2/Hz)
LT 17.7 17.5 17.2 16.8 16.2
L Shell 8.1 7.1 6.1 5.0 3.9
hhmm 0530 0600 0630 0700 0730
2012 Nov 13

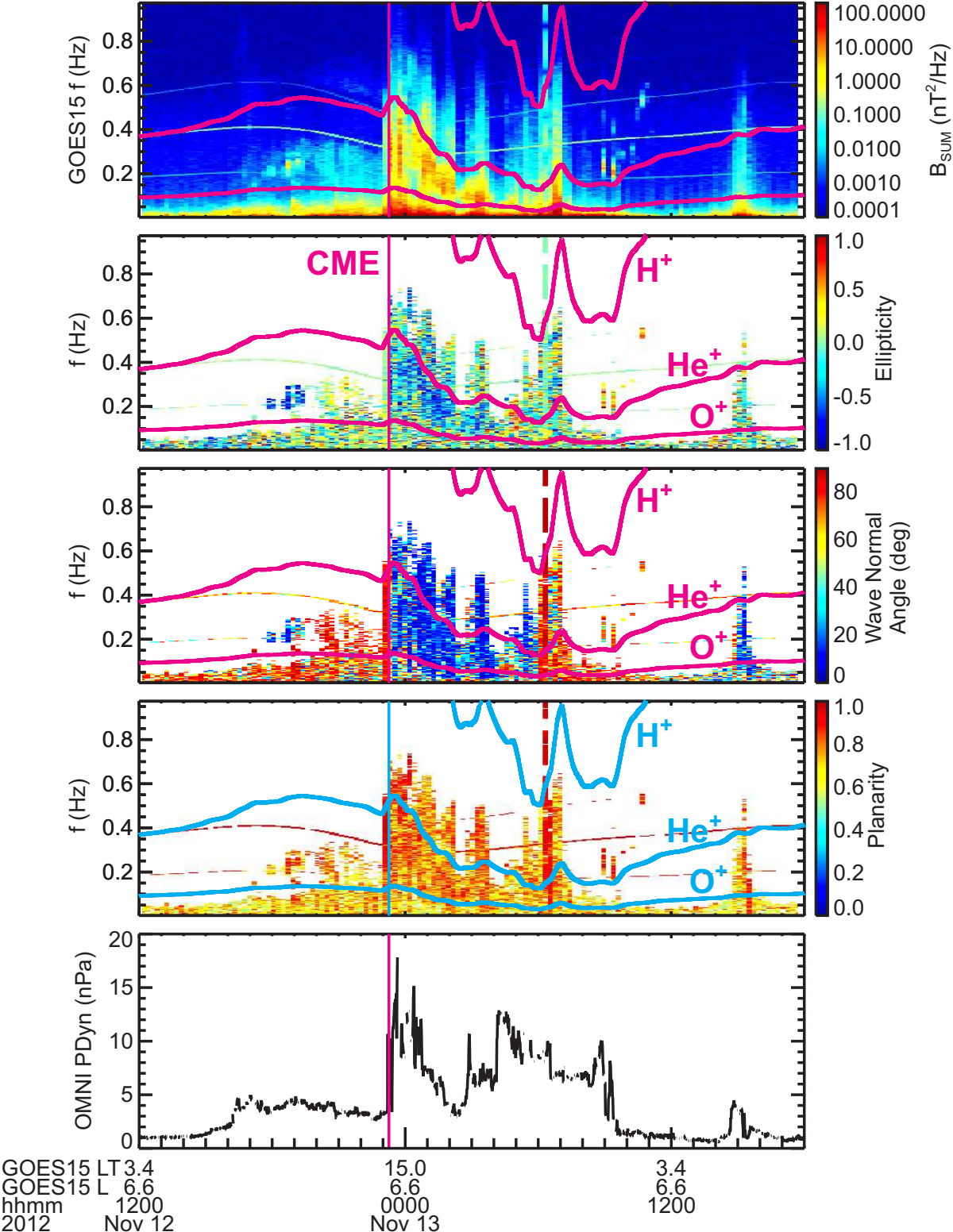
GOES15 f (Hz)
0.8
0.6
0.4
0.2
100.0000
10.0000
1.0000
0.1000
0.0100
0.0010
0.0001
B_SUM (nT²/Hz)
f (Hz)
CME
H+
He+
O+
1.0
0.5
0.0
-0.5
-1.0
Ellipticity
Wave Normal Angle (deg)
80
60
40
20
0
Planarity
OMNI PDyn (nPa)
20
15
10
5
0
GOES15 LT 3.4 15.0 3.4
GOES15 L 6.6 6.6 6.6
hhmm 1200 0000 1200
2012 Nov 12 Nov 13

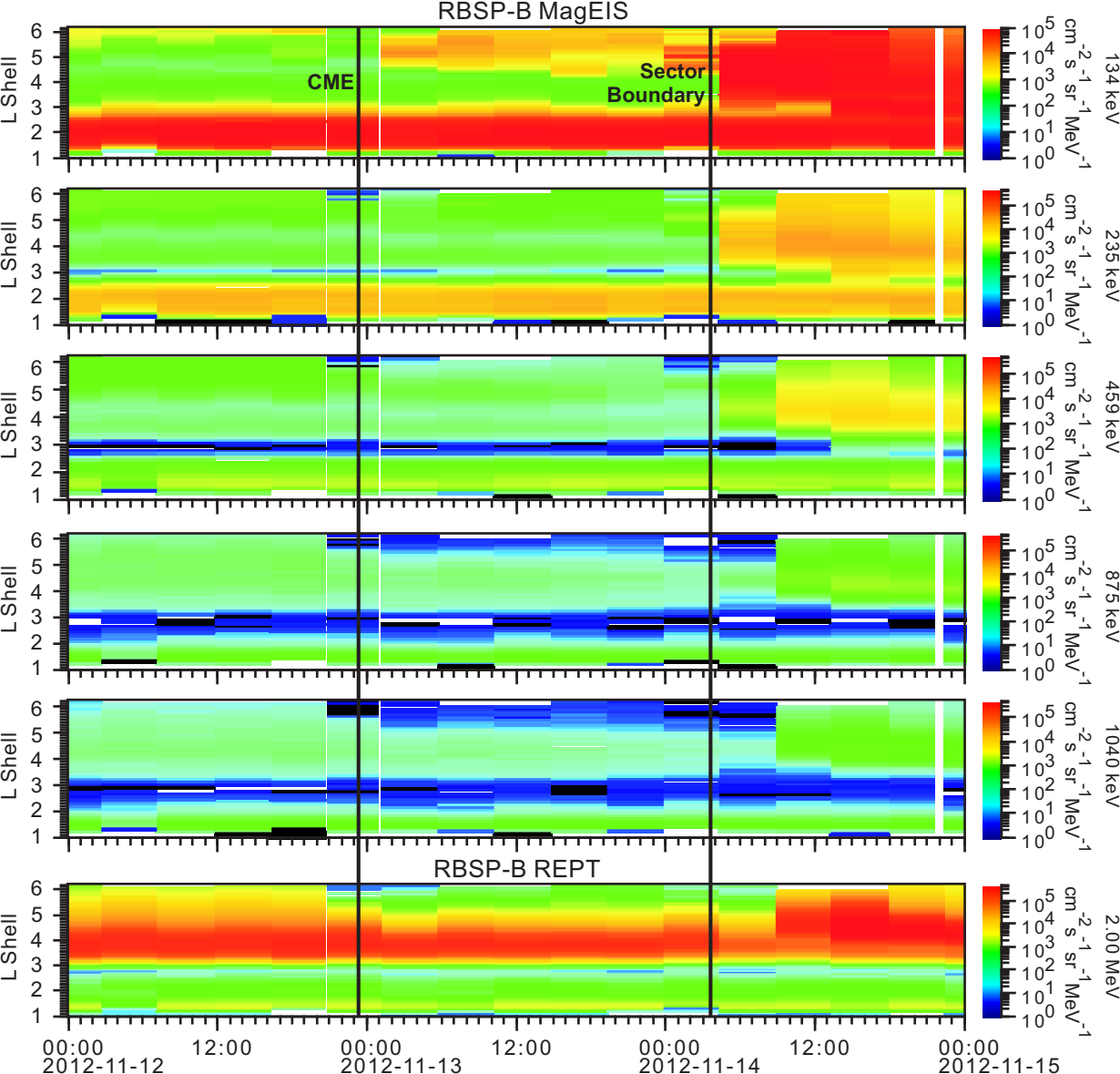
RBSP-B MagEIS
CME
Sector Boundary
L Shell
134 keV
235 keV
459 keV
875 keV
1040 keV
cm -2 s -1 sr -1 MeV -1
RBSP-B REPT
2.00 MeV
00:00 2012-11-12
12:00
00:00 2012-11-13
12:00
00:00 2012-11-14
12:00
00:00 2012-11-15